




Proteostasis is essential during cochlear development for neuron survival and hair cell polarity

Stephen Freeman^{1,†,*} , Susana Mateo Sánchez^{1,†}, Ronald Pouyo¹, Pierre-Bernard Van Lerberghe¹, Kevin Hanon¹, Nicolas Thelen¹, Marc Thiry¹, Giovanni Morelli^{1,2}, Laura Van Hees¹, Sophie Laguesse¹, Alain Chariot^{1,3,4}, Laurent Nguyen¹, Laurence Delacroix^{1,‡,**}  & Brigitte Malgrange^{1,‡,***} 

Abstract

Protein homeostasis is essential to cell function, and a compromised ability to reduce the load of misfolded and aggregated proteins is linked to numerous age-related diseases, including hearing loss. Here, we show that altered proteostasis consequent to Elongator complex deficiency also impacts the proper development of the cochlea and results in deafness. In the absence of the catalytic subunit Elp3, differentiating spiral ganglion neurons display large aggresome-like structures and undergo apoptosis before birth. The cochlear mechanosensory cells are able to survive proteostasis disruption but suffer defects in polarity and stereociliary bundle morphogenesis. We demonstrate that protein aggregates accumulate at the apical surface of hair cells, where they cause a local slowdown of microtubular trafficking, altering the distribution of intrinsic polarity proteins and affecting kinocilium position and length. Alleviation of protein misfolding using the chemical chaperone 4-phenylbutyric acid during embryonic development ameliorates hair cell polarity in Elp3-deficient animals. Our study highlights the importance of developmental proteostasis in the cochlea and unveils an unexpected link between proteome integrity and polarized organization of cellular components.

Keywords audition; ciliogenesis; microtubule; transport; tRNA-modifying enzyme

Subject Categories Cell Adhesion, Polarity & Cytoskeleton; Neuroscience; Protein Biosynthesis & Quality Control

DOI 10.15252/embr.201847097 | Received 18 September 2018 | Revised 13 June 2019 | Accepted 22 June 2019 | Published online 19 July 2019

EMBO Reports (2019) 20: e47097

Introduction

Sensorineural hearing loss, affecting millions of people worldwide, results from damage to the cochlear mechanosensory cells—i.e. the so-called hair cells (HCs)—or to their innervating spiral ganglion neurons (SGNs). There is increasing evidence that protein misfolding and aggregation are involved in hearing loss caused by environmental factors such as exposure to noise and ototoxic drugs [1]. Misfolded proteins are detrimental to cellular homeostasis because of their propensity to self-aggregate and aberrantly interact with other cellular components, disrupting normal cellular processes. Protein homeostasis (herein referred to as proteostasis) is reliant upon chaperones that assist protein folding or re-folding, and on their principal degradation systems, i.e. the ubiquitin–proteasome system and autophagy [2]. Polyubiquitinated proteins that fail to be degraded by the proteasome are transported along microtubules towards the microtubule-organizing centre (MTOC), where they gather to form a cytoprotective structure called an aggresome. Under pathological stress, these protein quality control systems can be overwhelmed and the accumulation of misfolded proteins can lead to cell death [3]. The ability to maintain proteostasis declines with age, and numerous age-related diseases have been linked to proteostatic disruption, including age-related hearing loss [4]. However, little is known about the importance of managing the proteome during the development of the auditory portion of the inner ear.

Most of the cells composing the cochlea derive from the otic placode, which consists of a thickened region of neuroectoderm. The SGNs are born early during development and start extending their peripheral processes towards the sensory epithelium (the organ of Corti, OC) before their target HCs have differentiated [5]. As the differentiation of HCs proceeds, these cells acquire dual levels of planar polarity, both of which are crucial for auditory

¹ GIGA-Neurosciences, Interdisciplinary Cluster for Applied Genoproteomics (GIGA-R), C.H.U. Sart Tilman, University of Liège, Liège, Belgium

² UHasselt, BIOMED, Hasselt, Belgium

³ GIGA-Molecular Biology of Diseases, Interdisciplinary Cluster for Applied Genoproteomics (GIGA-R), C.H.U. Sart Tilman, University of Liège, Liège, Belgium

⁴ Walloon Excellence in Life Sciences and Biotechnology (WELBIO), Wavre, Belgium

*Corresponding author. Tel: +32 4 3662178; E-mail: sdfreeman@protonmail.com

**Corresponding author. Tel: +32 4 3662178; E-mail: ldelaacroix@ulg.ac.be

***Corresponding author. Tel: +32 4 3665905; E-mail: bmalgrange@ulg.ac.be

[†]These authors contributed equally to this work as first, second authors

[‡]These authors contributed equally to this work as last authors

perception. Each HC develops a highly polarized mechanosensitive organelle at its apical surface to detect sound signals. This organelle is a v-shaped bundle of actin-rich microvilli (named stereocilia) that emerges in close association with the HC's specialized primary cilium (named the kinocilium). In addition to this cell-intrinsic planar polarity, all HCs are co-ordinately oriented in the plane of the epithelium—along the medio-lateral axis of the OC. This is referred to as “tissue planar polarity” and is most obviously indicated by the vertex of the stereociliary bundles pointing towards the lateral side of the epithelium. Both levels of polarity are dependent upon the asymmetric distribution of specific proteins in opposing medio-lateral domains [6]. Tissue planar polarity is governed by the so-called core planar cell polarity (PCP) proteins, which include Van Gogh-like (Vangl1 and Vangl2), Frizzled (Fz3 and Fz6) and Dishevelled [7–9]. Cell-intrinsic planar polarity is controlled by the asymmetric enrichment of GTP-binding protein alpha-I subunit 3 ($G\alpha_{i3}$), G-protein-signalling modulator 2 (GPSM2 or LGN), mammalian invertebrate (mInsc) and the atypical protein kinase C zeta (aPKC). These proteins have been shown to regulate mitotic spindle orientation in various tissues and organisms and are of crucial importance to centriole positioning from flies to mammals [10,11]. In the cochlear epithelium, these polarity proteins act to define the position of the kinocilium and the shape of the stereociliary bundle [12], which are crucial for normal audition [13].

Elongator is a highly conserved complex composed of duplicate copies of six subunits (Elp1–Elp6). Elp3 is the enzymatic core containing a lysine acetyltransferase motif and a radical S-adenosylmethionine (SAM) domain [14], but all subunits are required to serve the major function of the complex, which is to control translational efficiency via its regulation of tRNA modifications [15]. Elongator is the primary component of an enzymatic cascade that facilitates the addition of 5-methoxycarbonylmethyl and 5-carbamoylmethyl (mcm⁵ and ncm⁵, respectively) groups to the wobble uridine (U₃₄) in the anticodon of 11 different tRNAs [16]. These chemical modifications are essential to normal proteostasis, as they ensure high fidelity and speed of protein translation, and thus minimize the occurrence of protein misfolding [17,18]. In humans, mutations or genetic variations of genes encoding the various Elongator subunits have been linked to neurological disorders [19].

In the present study, we investigated the importance of proteostasis during cochlear development using conditional *Elp3* knockout mice (Elp3cKO) and chemical modulation of proteostasis. We found that protein misfolding and aggregation result in severe hearing loss by inducing apoptosis of SGNs and affecting

the establishment of HC intrinsic planar polarity. We show that the accumulation of protein aggregates at the apical surface of HCs interferes with vesicular transport along microtubules and alters the distribution of the proteins that control HC intrinsic planar polarity. Reducing the load of aggregates, through chemical chaperone treatment, restores HC intrinsic planar polarity although it is not sufficient to improve SGN survival. These results shed light on a new role for proteostasis during cochlear development, which is essential for normal hearing.

Results

Elp3 expression in the cochlea is essential for hearing

We analysed the temporal and spatial cochlear expression pattern of *Elp3* during embryonic and neonatal development using *in situ* hybridization and immunohistochemistry. *Elp3* mRNA is detected in the developing inner ear at embryonic day 12.5 (E12.5) in a ventro-medial region of the cochlear duct (CD) and in the cochleo-vestibular ganglion (CVG; Fig 1A). Later, we found *Elp3* transcripts are strongly expressed in the SGNs and in nascent HCs (Fig 1A, E16.5) and remain present in differentiated HCs in early postnatal animals (Fig 1A, P1). Immunofluorescent labelling of Elp3 protein at P1 confirmed this expression pattern (Fig 1B). Other proteins of the Elongator complex, such as Elp1, Elp5 and Elp6, are similarly expressed in the neonatal cochlea (Appendix Fig S1). To study the function of Elongator in inner ear development, we used a conditional knockout mouse line (Elp3lox/lox) [15], which when bred with the FoxG1: Cre transgenic line [20], resulted in the genetic ablation of *Elp3* in the otic vesicle from E8.5 onwards (conditional knockout mice are referred to as Elp3cKO from herein). The loss of *Elp3* expression in the cochlea of Elp3cKO mice was confirmed by *in situ* hybridization and Western blot (Fig 1C and D).

We initially noticed a potential hearing deficit in Elp3cKO mice when observing the Preyer's reflex in P19 animals, as none of them elicited a rapid movement of the body in response to a sharp hand-clap. We then recorded auditory brainstem responses (ABR) and confirmed this observation (Fig 1E and F). Sound-evoked potentials were observed from 35 to 40 decibels (dB) upwards in wild-type (WT) mice, whereas no neuronal activity could be recorded in Elp3cKO animals at all amplitudes tested, indicating profound hearing impairment (Fig 1E). Thus, conditional deletion of *Elp3* in the inner ear leads to deafness in mice.

Figure 1. Elp3 expression in the inner ear is essential for hearing.

- A *In situ* hybridizations for *Elp3* transcripts in the developing inner ear. Transcripts are present at E12.5 in a ventro-medial region of the developing cochlear duct (CD) and in the cochleo-vestibular ganglion (CVG). At E16.5, transcripts are present in the spiral ganglion neurons (SGNs) and in the newly formed hair cells (HCs) at the base of the cochlea, where they remain strongly expressed at P1. Scale bar = 50 μ m; inset = 25 μ m.
- B Elp3 specific immunostaining confirms the presence of the protein in HCs and SGNs at birth. Scale bar = 10 μ m.
- C, D Validation of Elp3 depletion from the cochlea in Elp3cKO animals. (C) At P1, Elp3 mRNA is absent from Elp3cKO. Scale bars = 50 μ m. *In situ* hybridizations were repeated four times. (D) Western Blots from P1 WT and Elp3cKO cochlear extracts confirm the loss of Elp3 at the protein level (cochleae from three different animals are pooled per sample).
- E Representative ABR recording from P19 WT and Elp3cKO animals reveals an absence of sound-evoked potentials in Elp3cKO animals, indicating that they suffer from severe hearing loss.
- F Elp3cKO animals present increased ABR thresholds (WT/Elp3cKO $n = 5/3$. Unpaired two-tailed t -test, $**P = 0.0017$, $t = 5.369$, $DF = 6$, mean \pm SD).
- Data information: #IHC; *OHC1; **OHC2; ***OHC3, OC: organ of Corti.

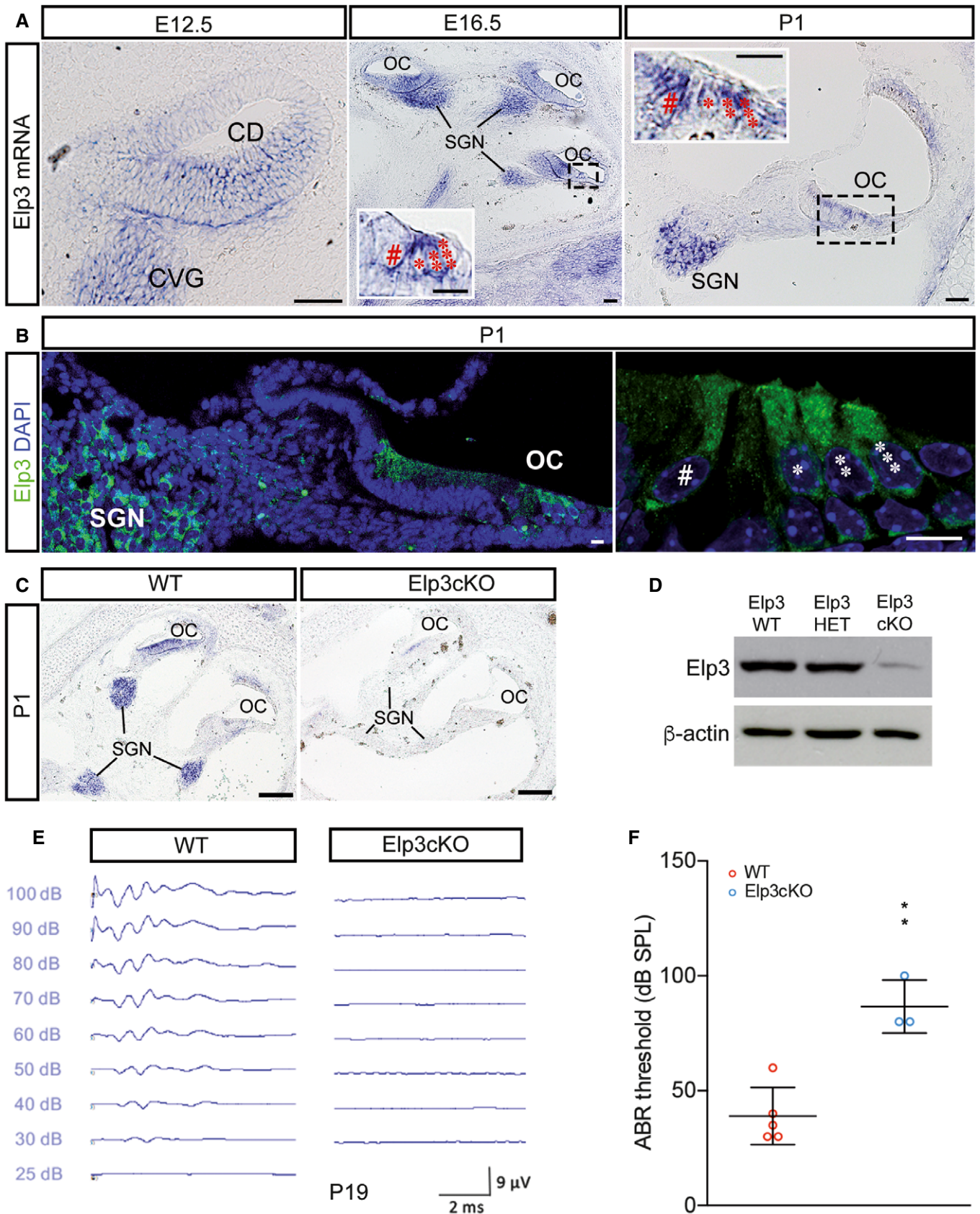


Figure 1.

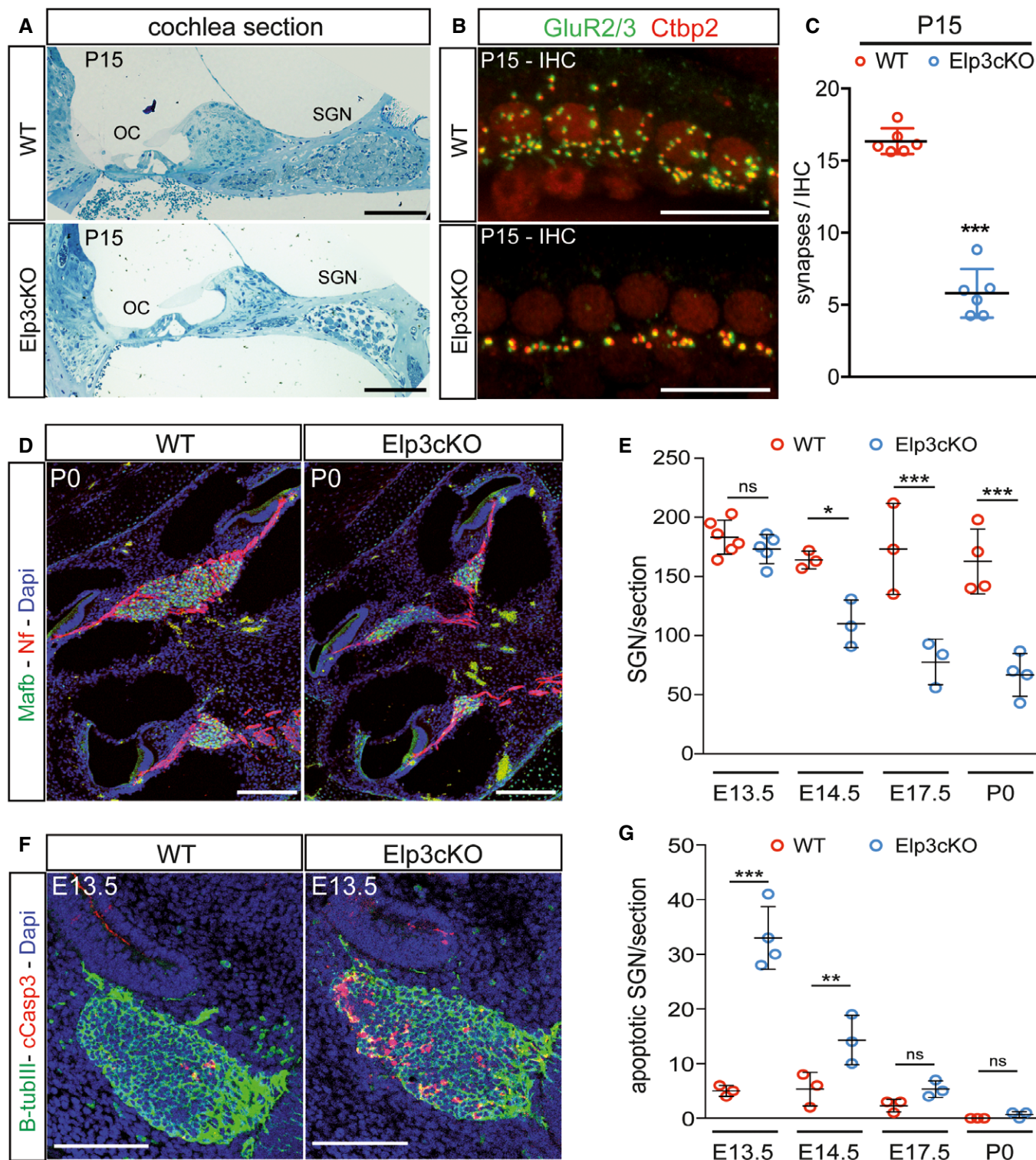


Figure 2.

Elp3 is crucial to spiral ganglion development

To investigate the possible causes of deafness upon *Elp3* depletion in the inner ear, we analysed semi-thin sections from P15 WT and *Elp3cKO* cochleae. While the organs of Corti showed no gross

abnormality, *Elp3*-depleted spiral ganglia were drastically reduced in size and SGN loss was obvious in all cochlear turns (Fig 2A). To assess if the remaining SGNs in *Elp3cKO* cochleae were still innervating their target cells at this stage, we performed specific labelings of the pre- and post-synaptic markers of the ribbon synapses,

Figure 2. Elp3cKO SGNs are lost before birth as a result of early apoptosis.

- A Toluidine blue stainings of semi-thin sections from P15 WT and Elp3cKO cochleae reveal a drastic reduction in the size of the spiral ganglion due to SGN loss. Scale bar = 100 μ m, OC: organ of Corti.
- B Specific labellings of the pre-synaptic marker Ctbp2 (in IHCs) and the post-synaptic marker GluR2/3 (in SGN terminals) indicate a decrease in the number of double-labelled dots in P15 Elp3cKO whole-mounted cochlea compared to WT. The remaining synapses still show coupling of the pre- and post-synaptic markers, suggesting they may be functional. Scale bar = 20 μ m.
- C The mean number of Ctbp2-GluR2/3 double-positive dots in IHCs from the basal region of P15 Elp3cKO cochleae is reduced by 65% compared to control ($n = 6$ animals per genotype; unpaired two-tailed t -test, $***P < 0.001$, $t = 13.48$, $DF = 10$, mean \pm SD).
- D NF-1 and MafB stainings on P0 cochlear sections indicate that SGN loss occurs before birth in Elp3cKO cochleae. Scale bar = 100 μ m.
- E SGN quantifications on cochlear sections from different embryonic stages reveal a loss of SGNs from E14.5 onwards ($n = 3$ –6 animals; one-way ANOVA, Tukey's multiple comparisons test; $***P < 0.001$; $*P < 0.05$; $F = 20.43$; $DF = 7$; mean \pm SD).
- F Detection of apoptotic SGNs from E13.5 cochlear sections with cleaved caspase-3 and B-tubIII stainings. Scale bar = 100 μ m.
- G The number of apoptotic SGN per section is significantly increased in E13.5 and E14.5 Elp3cKO compared to WT cochleae, suggesting SGNs are properly specified but die during their differentiation process ($n = 3$ –4 animals; one-way ANOVA, Tukey's multiple comparisons test; $***P < 0.001$; $**P < 0.01$; $F = 23.74$; $DF = 7$; mean \pm SD).

Ctbp2 and glutamate receptor GluR2/3, respectively (Fig 2B). In the absence of Elp3, Ctbp2 and GluR2/3 were still in close apposition in inner HCs (IHCs), suggesting the synapses may be functional. However, the number of these synapses was decreased by 65% when compared to control IHCs (Fig 2C), thus confirming massive SGN loss upon Elp3 depletion. In order to evaluate the temporal window of neuronal loss, we counted Gata3 or MafB-labelled SGN nuclei on WT and Elp3cKO cochlear sections at different stages of embryonic development (Fig 2D and E). While the mean number of neurons was similar at E13.5 for Elp3cKO and controls, it was significantly reduced upon Elp3 invalidation at all later stages. At birth, the SGN population in Elp3cKO cochleae was decreased by 59% compared to controls (Fig 2E). These results suggest that SGNs are correctly specified but subsequently die during their differentiation. Therefore, we next checked for markers of apoptosis by performing cleaved caspase-3 labelling on cochlear sections. We observed a significant increase in the number of apoptotic SGNs in Elp3cKO cochleae at E13.5 and E14.5 (Fig 2F and G). Altogether, these results show that Elp3 ensures SGN survival at early stages of development.

Elp3 deficiency is associated with the presence of aggresome-like structures in the developing SGNs and HCs

Loss of Elp3 is known to cause inefficient decoding by tRNAs lacking U_{34} modification and to increase the frequency of protein misfolding and aggregation [18]. Since neurons are particularly vulnerable to proteotoxic stress [21], we reasoned that SGN

apoptosis in Elp3cKO could be a consequence of unresolved protein aggregation. Thus, we checked for the presence of aggregates in SGNs at E13.5, immediately before SGN number begins to fall in Elp3cKO cochleae.

Using the PROTEOSTAT[®] aggresome detection kit, we observed an intense labelling in SGNs of E13.5 Elp3cKO cochleae (Fig 3A). To confirm this finding, we performed transmission electron microscopy (TEM) and identified cells harbouring large electron dense structures that distort the shape of the cell nucleus (Fig 3B). We observed that these structures are not enclosed by a membrane, further confirming that they present typical aggresome characteristics [22]. These results demonstrate that proteostasis is heavily compromised in Elp3-deficient SGNs, as misfolded proteins have accumulated to form large juxtannuclear aggresome-like structures.

Abnormal amounts of misfolded proteins are known to activate the unfolded protein response (UPR). This adaptive response induces cellular chaperones, increases proteasomal and autophagy capacities and reduces the rate of protein synthesis. However, if these programmes are not sufficient to alleviate the load of misfolded proteins, UPR can induce apoptosis by upregulating Chop transcription factor [3] and its target gene *Chac1* [23]. Hence, we performed RT-qPCR analysis on E14.5 control and Elp3cKO cochleae and found a significant increase in *Chop* and *Chac1* transcripts in the absence of Elp3 (Fig 3C), suggesting that the pro-apoptotic arm of UPR is induced in response to compromised protein homeostasis. Collectively, these results demonstrate that SGNs survival during embryonic stages of cochlear development is reliant on Elp3 to ensure proteome integrity.

Figure 3. Aggresome-like structures are formed in SGNs and HCs from Elp3cKO animals.

- A Proteostat staining of WT and Elp3cKO E13.5 cochlear sections reveals the presence of numerous aggresome-like structures in Elp3-deficient SGNs. Scale bar = 100 μ m.
- B Transmission electron micrographs from E13.5 Elp3cKO SGNs confirm the presence of apoptotic neurons (marked by a red arrowhead) and a large electron dense juxtannuclear structure typical of aggresomes (dashed circle). Scale bars = 10 and 2 μ m (last panel).
- C Chop and Chac1 transcripts are upregulated in E14 Elp3cKO compared to WT cochleae ($n = 8/6$ for WT/KO; unpaired t -test two-tailed; $P = 0.0001/0.0015/0.0010$; $t = 9.535/4.090/4.307$; $DF = 12/12/12$ for Elp3, Chop and Chac1 respectively; mean \pm SEM presented), indicating that the pro-apoptotic arm of the unfolded protein response (UPR) is activated in Elp3-deficient SGNs.
- D, E Proteostat staining of whole-mounted P0 organs of Corti reveals the presence of aggregates in HCs upon loss of Elp3. Orthogonal slices (Orthog) reveal aggregated proteins localize at the apical surface of Elp3cKO HCs. Scale bars = 5 μ m. [#]IHC; *OHC1; **OHC2; ***OHC3.
- F Protein extracts from P1 cochleae show increased levels of polyubiquitinated conjugates upon loss of Elp3, confirming proteostasis disruption.
- G The levels of Chop and Chac1 transcripts are unaffected by Elp3 depletion in P0 organs of Corti ($n = 3$ animals per genotype; unpaired t -test two-tailed; $P = 0.0003/0.4296/0.056$; $t = 11.62/0.8778/2.662$; $DF = 4/4/4$ for Elp3, Chop and Chac1 respectively; mean \pm SEM presented), suggesting that proteostasis disruption in Elp3cKO HCs is not sufficient to induce UPR-mediated apoptosis.

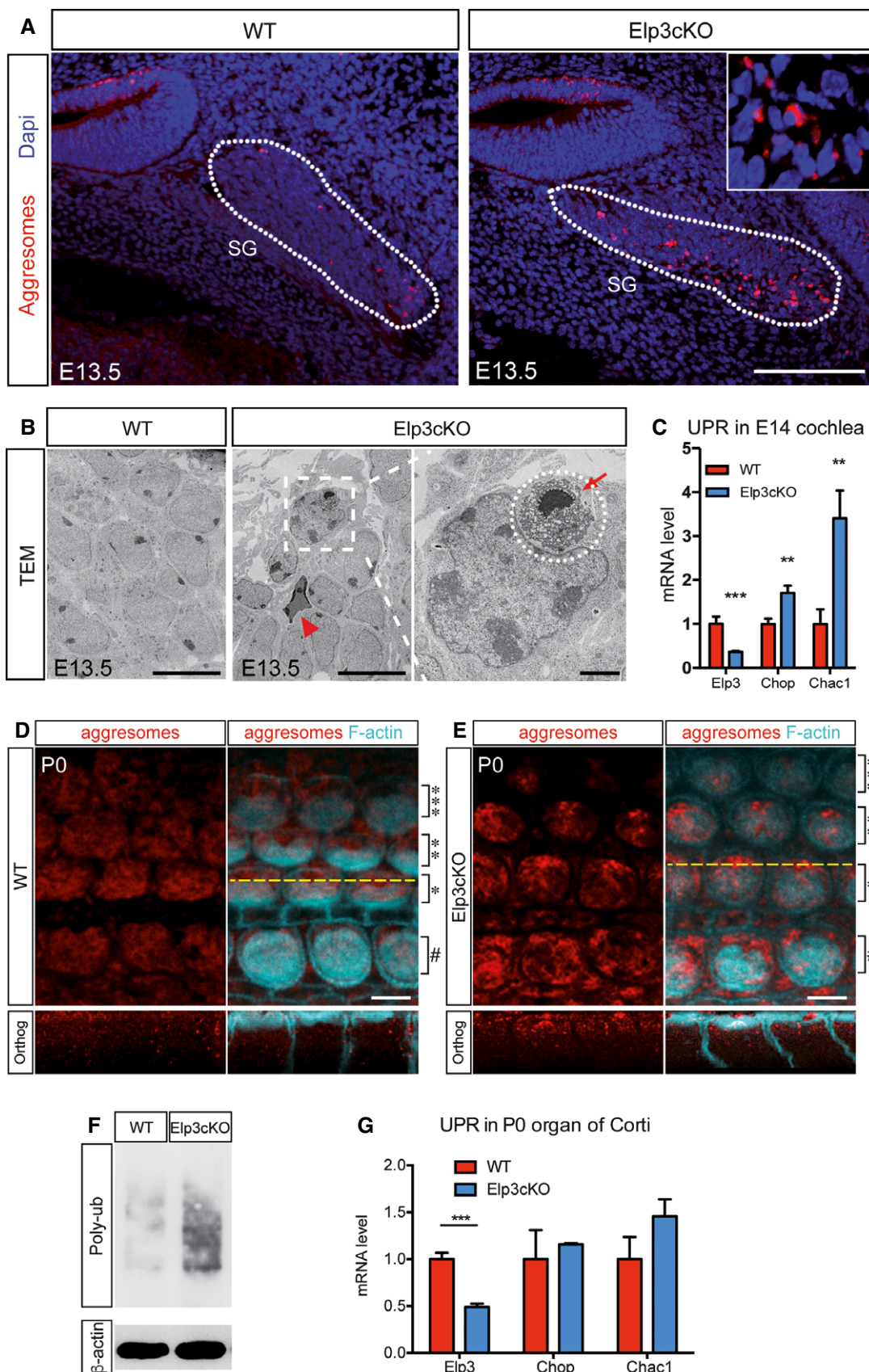


Figure 3.

As *Elp3* is expressed in the auditory HCs (Fig 1B), we next investigated whether aggresome-like structures would also be present in HCs of *Elp3cKO* animals. By performing PROTEOSTAT[®] staining, we detected protein aggregates that accumulate predominantly in the most apical portion of P0 HCs (Fig 3D and E, orthog). In addition, we found that the level of polyubiquitinated conjugates is drastically increased in neonatal *Elp3cKO* cochlea (Fig 3F). This confirms that the extent of misfolded and aggregated proteins exceeds the capacity of the cells to degrade them. Interestingly, proteostasis disruption in *Elp3cKO* HCs was not sufficient to activate the pro-apoptotic arm of UPR, as *Chop* and *Chac1* transcript levels in neonatal OC were similar than those of controls (Fig 3G). Altogether, our results indicate that *Elp3* is crucial to proteome integrity in the developing cochlea but that SGNs and HCs respond differently to protein homeostasis impairment.

Elp3cKO HCs exhibit defective polarity and ciliogenesis

Scanning electron microscopy (SEM) of P19 cochleae revealed that HCs are able to survive to proteostasis disruption in *Elp3cKO*s, as none of them are missing (Fig 4A). However, the polarity of the auditory epithelium appeared to be affected by the absence of *Elp3* as some stereociliary bundles protruding from the apical surface of HCs displayed modest alterations in morphology and orientation (Fig 4A, indicated by arrowheads and arrows, respectively) when compared to controls. Actin stainings of P1 cochleae revealed that the polarity defects were more pronounced at birth, as some actin-rich bundles in *Elp3cKO* were misoriented along the medio-lateral axis and many of them appear flatter than those of WT (Fig 4B).

We first evaluated the defects observed at the level of tissue polarity by quantifying the angle formed between the stereociliary bundle and the medio-lateral axis of the epithelium at birth. We

found a broader distribution in the last two rows of outer HCs (OHCs) in *Elp3cKO* as compared to WT littermates (Fig 4C). This mild tissue planar polarity defect was accompanied by a slight reduction of the cochlear length (Appendix Fig S2A–C) and an extended region of mispatterned HCs in the apical turn (Appendix Fig S2D and E). However, it was not associated with alterations in the polarized localization or the expression level of core PCP proteins *Vangl2* and *Fz6* (Appendix Fig S3A–E).

We next evaluated the intrinsic polarity of HCs from *Elp3cKO* cochleae, as most of them possessed a flatter bundle (Fig 4A, B and D). Indeed, we found that the angle formed by the stereociliary bundle was significantly larger in all three rows of OHCs in neonatal *Elp3cKO* mice as compared to WT (Fig 4E). To analyse the positioning of the bundle, we measured the area of the two compartments of the HC apical surface that abut the stereocilia—the lateral “bare zone”, so called as it is devoid of microvilli, and the medial zone (see Fig 4F). Although the apical surface areas of WT and *Elp3cKO* HCs were comparable (Appendix Fig S4), *Elp3cKO* HCs had a larger bare zone and a smaller medial zone, revealing that their stereociliary bundles were more centrally positioned (Fig 4F and G).

The development of the stereociliary bundle is tightly linked to the formation and positioning of the kinocilium, which, after emerging from a central region of the HC apical surface at E15.5, migrates and localizes near the lateral edge of the cell [24,25]. We thus analysed the length and position of kinocilia in P0 animals. The kinocilia of OHCs were significantly shorter in *Elp3cKO* cochleae as compared to WT (Fig 4H). Positional plotting revealed *Elp3cKO* kinocilia to be abnormally scattered both in IHCs and OHCs. In OHCs of *Elp3cKO* animals, kinocilia were significantly displaced medially (Fig 4I).

Disruptions in the localization of intrinsic polarity proteins can result in flatter, misshaped stereociliary bundles, displaced kinocilia and mild tissue planar polarity defects [12,26]. Thus, we next

Figure 4. *Elp3* is necessary for embryonic establishment of HC polarity and ciliogenesis.

- A Scanning electron micrographs of cochlear tissue from P19 animals indicate no HC loss in the absence of *Elp3* but illustrate some defects of polarity, as misaligned HCs and dysmorphic stereociliary bundles are visible (red arrows and white arrowheads, respectively). Scale bars = 5 μ m.
- B Surface view of P1 actin-stained organ of Corti confirms defective establishment of polarity in *Elp3cKO* as numerous stereociliary bundles are misaligned along the medio-lateral axis (M-L) or misshaped. Scale bars = 5 μ m.
- C *Elp3cKO*s exhibit a broader distribution of hair cell orientation. The angles of deviation between the stereociliary bundle and the medio-lateral axis are plotted in rose diagrams, for each OHC row. Whereas the majority of WT bundles are pointing to the most lateral region of the tissue (within a range of 10°), many *Elp3cKO* bundles of the two last rows of OHCs present increased angles of deviation (WT/*Elp3cKO* OHC1: $n = 99/99$, $P > 0.1$, DF = 99; OHC2: $n = 99/100$, $P < 0.001$, DF = 99; OHC3: $n = 99/98$, $P < 0.001$, DF = 98; pooled data from six animals per genotype; Watson U^2 test).
- D–G *Elp3cKO*s HCs harbour a flatter stereociliary bundle that is centrally shifted. (D) Scanning electron micrographs of HCs from P1 WT and *Elp3cKO* cochleae (scale bar = 2 μ m) illustrating the misshaped stereociliary bundles and the shorter kinocilium (false coloured in pink) of *Elp3cKO* HCs. (E) Graph presents the mean angle of HC bundle ($n = 6$ animals; one-way ANOVA, Tukey's multiple comparisons test; $***P < 0.001$, $F = 13.69$, DF = 7; mean \pm SD). (F) *Elp3cKO* HCs possess a significantly larger bare zone (WT/KO IHC: $n = 23/24$ cells; OHC1: $n = 27/27$; OHC2: $n = 27/29$; OHC3: $n = 30/29$; cumulative data collected from three animals per genotype; one-way ANOVA, Tukey's multiple comparisons test; $***P < 0.001$, $*P < 0.05$, $F = 16.72$, DF = 7; mean \pm SD). (G) *Elp3cKO* HCs possess a significantly smaller medial zone (WT/KO IHC: $n = 23/24$ cells; OHC1: $n = 27/27$; OHC2: $n = 27/29$; OHC3: $n = 27/29$; cumulative data collected from three animals per genotype; one-way ANOVA, Tukey's multiple comparisons test; $***P < 0.001$, $*P < 0.05$, $F = 63.3$, DF = 7; mean \pm SD).
- H Kinocilia are shorter in *Elp3cKO* HCs (WT/KO IHC: $n = 15/15$; OHC1: $n = 30/32$; OHC2: $n = 31/30$; OHC3: $n = 27/30$; data collected from three animals per genotype; one-way ANOVA, Tukey's multiple comparisons test, $***P < 0.001$, $**P < 0.01$, $F = 19.6$, DF = 7; mean \pm SD).
- I High magnification of representative HCs from P1 WT and *Elp3cKO* cochleae stained for F-actin and gamma tubulin (white). The basal body of kinocilia is shifted centrally at the apical surface of *Elp3cKO* HCs. Scale bars = 2 μ m. Polar plotting of kinocilium basal body position for each row of HCs of WT and *Elp3cKO* (WT/KO IHC: $n = 42/32$; OHC1: $n = 47/48$; OHC2: $n = 47/45$; OHC3: $n = 44/44$; cumulative data collected from three animals per genotype). Cellular orientations were tested using Watson U^2 test ($P < 0.001$ between WT/*Elp3cKO*, for all HC rows) and the mean vector lengths, determined from the cell centre to the basal body, were compared using t -tests ($P < 0.001$ between WT/*Elp3cKO*, for all HC rows).
- J–L The localization of apical polarity proteins is affected by *Elp3* loss. Surface views of mid-basal turn of P1 cochleae from WT or *Elp3cKO* mice stained with LGN (J), $G\alpha_3$ (K) or aPKC (L) and F-actin. The enrichment of these apical polarity regulators at the lateral (J, K) and medial (L) edges of HCs is disrupted in *Elp3cKO* HCs. Scale bars = 5 μ m (upper panels) and 2 μ m (lower panels).

Data information: #IHC; *OHC1; **OHC2; ***OHC3.

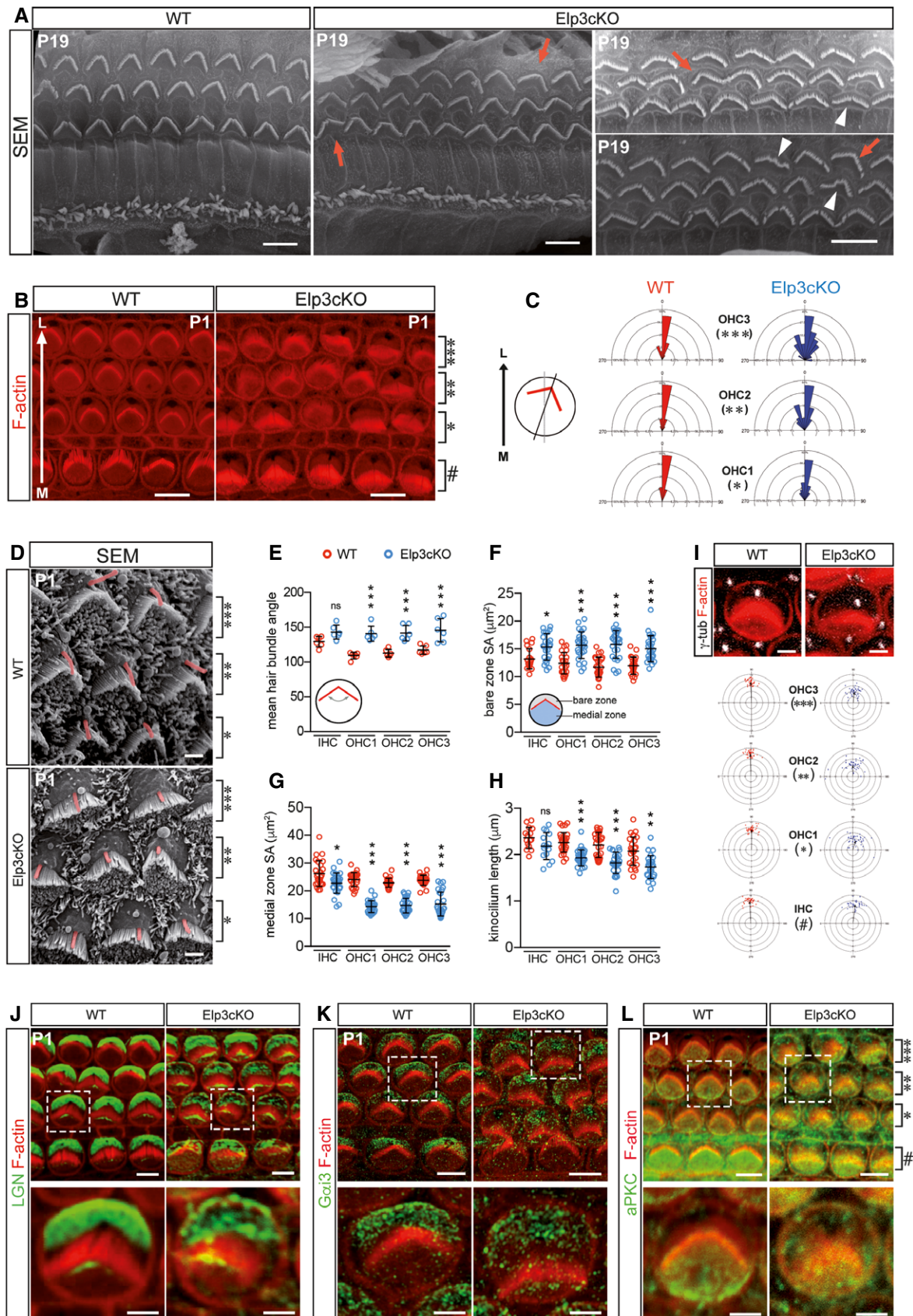


Figure 4.

sought to analyse the distribution of the intrinsic polarity proteins $G\alpha_{13}$, LGN and aPKC. In neonatal HCs of control animals, LGN and $G\alpha_{13}$ are localized exclusively at the lateral side of HCs (Fig 4J and K), where they collectively exclude aPKC [12], forcing it to occupy the opposite medial region (Fig 4L). In the absence of Elp3, LGN and $G\alpha_{13}$ are still polarized to the lateral domain, but they occupy a larger area and display a less homogenous distribution (Fig 4J and K). Strikingly, the medial restriction of aPKC is lost in the absence of Elp3, as it is also present in the lateral domain of the HC apical surface (Fig 4L).

Altogether, these data suggest that embryonic expression of Elp3 is necessary for multiple components of HC intrinsic polarity, which includes the organization of the stereociliary bundle, the location of the kinocilium and the distribution of intrinsic polarity proteins.

Intrinsic polarity is dependent upon Elongator's function on tRNAs and is impaired upon aggresome formation

We next sought to investigate whether Elongator deficiency could perturb the distribution of intrinsic polarity proteins in other cellular contexts. These proteins are also associated with the regulation of mitotic spindle orientation during cell division, where their polarized enrichment at the cell cortex exerts pulling forces on astral microtubules [10,27]. Thus, we tested if Elp3 suppression could disrupt the localization of polarity proteins in dividing cells. Validated siRNA-treated HEK293T cells (Appendix Fig S5A) were immunolabelled for LGN and acetylated alpha-tubulin. LGN accumulates at the cell cortices in mitotic HEK293T cells treated with control siRNA, but this cortical enrichment is disrupted in siElp3-transfected cells (Fig 5A and B). Interestingly, we also observed perturbations in ciliogenesis since non-dividing siElp3-transfected HEK293T cells harbour shorter primary cilia (Fig 5C and D).

We then analysed the effects of silencing *Alkbh8* (Appendix Fig S5A), the enzyme responsible for the final step of mcm^5/ncm^5 U_{34} modification of tRNAs. The cortical enrichment of LGN was severely disrupted in dividing *Alkbh8*-depleted HEK293T cells (Fig 5A and B), and furthermore, the length of their primary cilia was significantly reduced (Fig 5C and D). Knockdown of the Elongator

subunits Elp1 and Elp5 caused a similar disruption of LGN cortical enrichment (Appendix Fig S5B–D), indicating that the process is controlled by the Elongator holo-enzyme. Collectively, these results indicate that the establishment of polarity and ciliogenesis is reliant on proper tRNA modifications and likely dependent upon proteome homeostasis since the lack of U_{34} modification increases the frequency of protein misfolding [18]. Accordingly, we confirmed that siElp3- and siAlkbh8-transfected HEK293T contained elevated levels of polyubiquitinated conjugates and aggresome-like structures compared to control cells (Fig 5E–G).

We next wondered whether disrupting proteostasis in an Elongator-independent manner could also impair LGN distribution. For this purpose, we cultured HEK293T cells in the presence of the proteasome inhibitor MG-132 and found that the accumulation of protein aggregates resulted in LGN mislocalization during mitosis (Fig 5H and I). Strikingly, the HCs of cochleae treated with MG-132 possessed apically localized aggregates that were highly reminiscent of those observed in the *Elp3* cKO cochlea (Fig 5J). The presence of aggregates was accompanied by apical polarity disruption, as MG-132-treated HCs displayed impaired localization of LGN and misshaped stereociliary bundles (Fig 5K). Together, these data show that the presence of protein aggregates is responsible for the mislocalization of intrinsic polarity proteins.

Misfolded protein accumulation causes a reversible slowdown of microtubular transport

We next explored the mechanisms underlying the disruption of intrinsic polarity protein distribution upon aggresome formation. We first checked for LGN and $G\alpha_{13}$ protein levels and found no significant differences in *Elp3*-deficient HEK293T or neonatal cochleae compared to controls (Fig 6A and B). As we found a spatial association between the apical polarity proteins and the aggresome-like structures, we checked whether they could be particularly prone to protein aggregation by performing co-immunolabelings for LGN or $G\alpha_{13}$ and aggresomes in HEK293T cells. We observed that neither LGN nor $G\alpha_{13}$ is found in aggregates induced by *Elp3* suppression (Fig 6C).

Figure 5. Intrinsic polarity is dependent upon Elongator's function on tRNAs and is impaired upon proteasome inhibition.

- A, B Polarized enrichment of LGN at the cortices of dividing HEK293T cells is disrupted upon *Elp3* or *Alkbh8* knockdown. (A) HEK293T cells transfected with siRNAs for *Elp3*, *Alkbh8* or control and immunolabelled with LGN, acetylated alpha-tubulin and DAPI. Scale bar = 5 μ m. (B) The mean fluorescence intensity profile of LGN across the radii perpendicular to division in HEK293T cells was quantified (siRNA control/*Elp3*/*Alkbh8*: $n = 27/30/27$; pooled from three independent experiments; mean \pm SEM).
- C, D The length of the primary cilium is reduced in non-dividing HEK293T cells upon *Elp3* or *Alkbh8* knockdown. (C) Control, *Elp3* or *Alkbh8* siRNA-treated HEK293T cells were immunolabelled for basal body marker ALMS1, axoneme marker Arl13b and DAPI. Scale bar = 5 μ m. (D) Primary cilium length of non-dividing HEK293T was measured, and pooled data were plotted (siRNA control/*Elp3*/*Alkbh8*: $n = 94/81/90$; data collected from three independent experiments; one-way ANOVA, Tukey's multiple comparisons test, $***P < 0.001$, $F = 21.46$, $DF = 4$; minimum, first quartile, median, third quartile and maximum presented).
- E, F *Elp3* knockdown increases the amount of polyubiquitinated conjugates in HEK293T cells ($n = 3$; one-way ANOVA, Tukey's multiple comparisons test, $**P < 0.01$, $*P < 0.05$, $F = 16.51$, $DF = 2$; mean \pm SD).
- G Increased formation of aggresome-like structures in *Elp3*- or *Alkbh8*-depleted HEK293T. Aggresomes (red); DAPI (blue). Enlarged images depict examples of non-dividing (left) and dividing (right) cells. Scale bar = 10 μ m.
- H, I Inducing aggresomes with MG-132 disrupts the polarized enrichment of LGN at the cortices of dividing HEK293T cells. (H) HEK293T cells treated with DMSO vehicle or MG-132 and stained for aggresomes (left panels) or LGN, F-actin and DAPI (green, red and blue, respectively, in right panels). Scale bar = 10 μ m. (I) Fluorescence intensity profile of LGN across the radii perpendicular to division in dividing HEK293T cells. Mean fluorescence values per percentage of cell length with SEM are plotted. Fluorescence intensity profiles collected from three independent experiments (DMSO/MG-132: $n = 24/24$).
- J Proteostat staining of MG132-treated whole-mounted PO organs of Corti reveals the presence of aggresome-like structures in HCs. Orthogonal slices (Orthog) reveal aggregated proteins localize at the apical surface of MG132-treated HCs. Scale bars = 5 μ m. #IHC; *OHC1; **OHC2; ***OHC3.
- K Localization of LGN at the lateral apical surface of E16.5 WT HCs is disrupted by MG-132. LGN (white/green) and F-actin (red). Scale bars = 5 μ m; magnified views = 2 μ m.

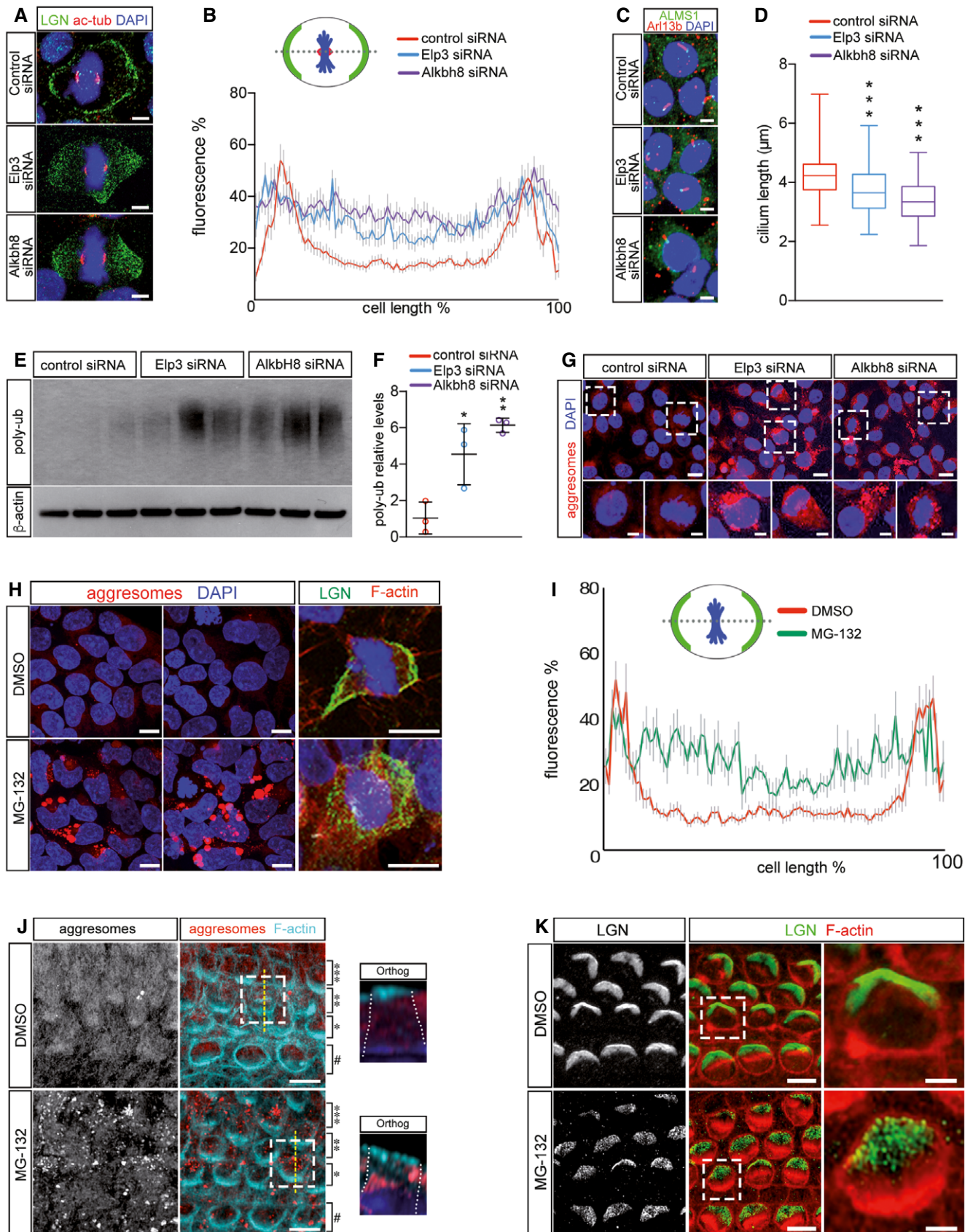


Figure 5.

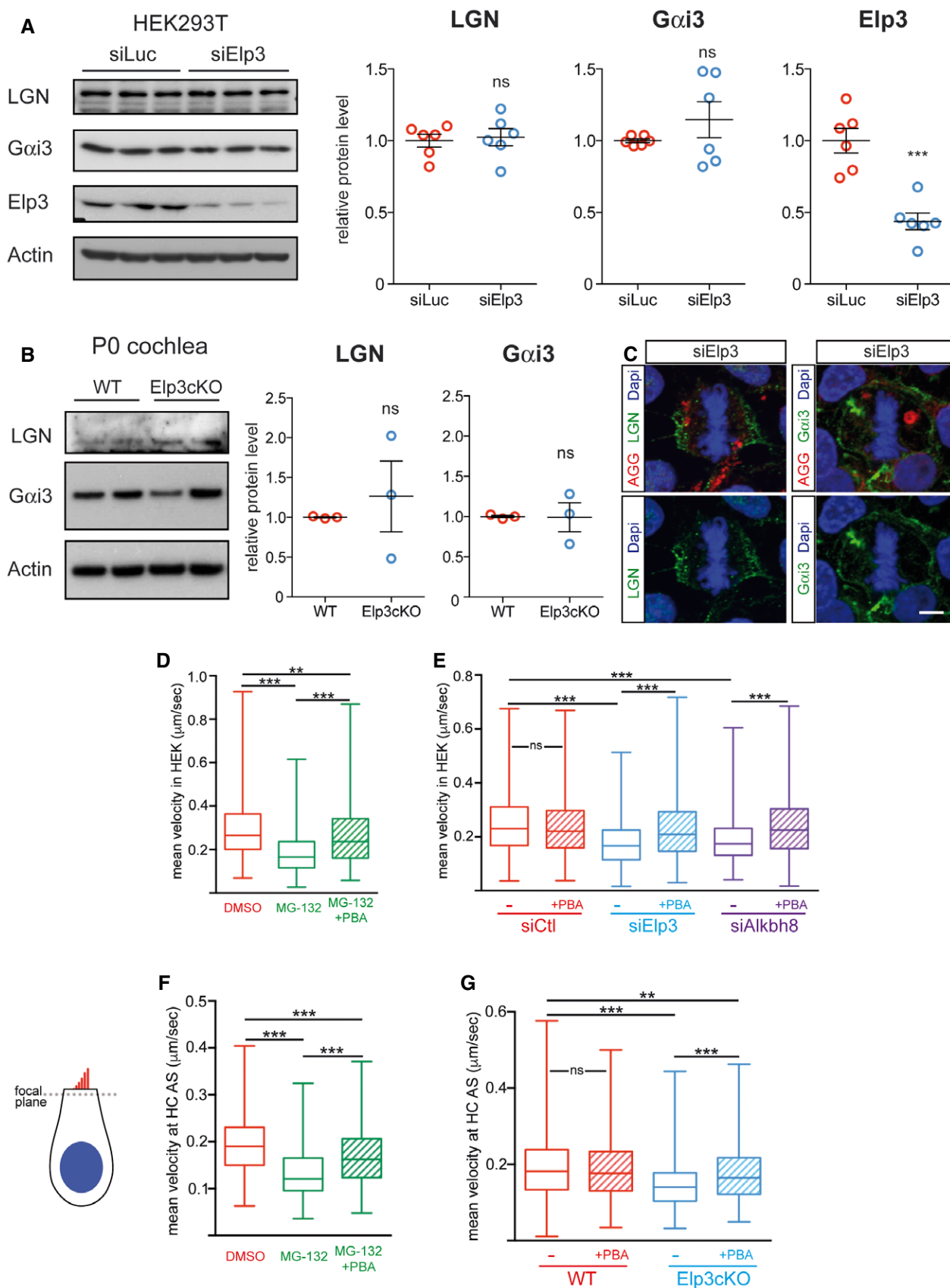


Figure 6.

Figure 6. The presence of aggresome-like structures affects microtubular transport speed in cultured HEK293T cells and cochlear HCs.

A, B LGN and $G\alpha_{13}$ protein levels are not affected by Elp3 loss. (A) Western blots with total lysates from control and Elp3 siRNA-treated HEK293T cells and corresponding quantifications of normalized LGN, $G\alpha_{13}$ and Elp3 levels ($n = 6$ from two independent cultures; unpaired two-tailed t -test, LGN: $P = 0.749$, $t = 0.328$, $DF = 10$, $G\alpha_{13}$: $P = 0.275$, $t = 1.155$, $DF = 10$, Elp3: $***P = 0.0003$, $t = 5.438$, $DF = 10$, mean \pm SEM). (B) Western blots on P0 WT and Elp3cKO cochlear extracts and corresponding quantifications of normalized LGN and $G\alpha_{13}$ levels ($n = 3$, each lysate obtained from cochleae pooled from two animals; unpaired two-tailed t -test, LGN: $P = 0.586$, $t = 0.591$, $DF = 4$, $G\alpha_{13}$: $P = 0.963$, $t = 0.0491$, $DF = 4$, mean \pm SEM).

C Mislocalized LGN and $G\alpha_{13}$ are not found in protein aggregates formed upon Elp3 depletion. HEK293T cells transfected with Elp3 siRNA were co-stained for aggresomes, Dapi and LGN or $G\alpha_{13}$. Scale bar = 5 μ m.

D–G Microtubular transport speed is reduced by the presence of aggresome-like structures in HEK293T cells and cultured HCs and is improved upon 4-PBA treatment. The mean velocity of lysosomes was measured on time-lapse recordings of HEK293T cells (D, E) and HCs, at the level of their apical surface (F, G), labelled with LysoTracker®. (D): DMSO/MG-132/MG-132 + 4PBA $n = 555/337/453$, pooled from three experiments, $***P < 0.001$, $**P < 0.01$. (E): siCtl/+4PBA $n = 622/677$; siElp3/+4PBA $n = 674/577$; siAlkbh8/+4PBA $n = 460/484$, pooled from four experiments, $***P < 0.001$. (F): DMSO/MG-132/MG-132 + 4PBA $n = 210/225/266$, pooled from three experiments, $***P < 0.001$. (G): WT/WT + 4PBA/Elp3cKO/Elp3cKO + 4PBA $n = 732/763/730/738$, pooled from four OCs per condition, $***P < 0.001$, $**P < 0.01$. All data analysed with Kruskal–Wallis ANOVA, Dunn's multiple comparisons test. Box/whisker plots depict minimum, first quartile, median, third quartile and maximum.

We then asked whether aggresome-like structures could affect intrinsic polarity proteins distribution by perturbing transport along microtubules, as it is known that following proteasome inhibition, movement of organelles is inhibited and microtubular transport is impaired [28]. By performing time-lapse recordings of HEK293T stained with LysoTracker®, we found that lysosomal transport was significantly reduced upon MG-132 treatment and Elp3 or Alkbh8 suppression compared to controls (Fig 6D and E).

We then used the well-characterized chemical chaperone 4-phenylbutyric acid (4-PBA) to improve protein folding and thus alleviate the load of cellular aggregates (Appendix Fig S6). In MG-132-, siElp3- or siAlkbh8-treated HEK293T cells, a co-treatment with 4-PBA improved transport speed, showing that microtubular trafficking could be ameliorated upon proteostasis restoration (Fig 6D and E).

We also generated *ex vivo* time-lapse recordings of lysosomal movement at the apical surface of HCs from cultured E16.5 OC. We found that the transport speed along microtubules was reduced upon proteasome inhibition by MG-132 (Fig 6F and Movies EV1 and EV2) and observed a similar slowdown in HCs from Elp3cKO compared to WT (Fig 6G and Movies EV3 and EV4). Interestingly, this reduction in velocity was specific to the apical surface of the HC and was not observed in mid-basal regions (Appendix Fig S7). Again, 4-PBA treatment induced a significant amelioration of transport along microtubules, demonstrating that the speed of moving vesicles is correlated with the load of misfolded protein aggregates (Fig 6F and G, and Movies EV5–EV7). Collectively, these results highlight the importance of proteostasis in the control of microtubular trafficking and suggest that the mislocalization of intrinsic polarity proteins we observed in Elp3-depleted or MG-132-treated cells is a consequence of their reduced trafficking along the microtubular cytoskeleton.

Alleviation of protein misfolding improves the establishment of intrinsic polarity in MG-132-treated and Elp3cKO HCs

Having identified that the chemical chaperone 4-PBA was able to counteract the effects of protein aggregation on microtubular transport speed, we next tested its effect on cochlear HC intrinsic planar polarity. We first analysed LGN distribution and kinocilium position in cultured OCs treated with MG-132. The accumulation of protein aggregates in MG-132 treated HCs altered the distribution of LGN

but co-treatment with 4-PBA improved its restricted localization as many HCs regain an intense crescent-shaped LGN enrichment at the lateral cortex, which is characteristic of its distribution in normal HCs (Fig 7A). Furthermore, MG-132 induced a central shift of the kinocilium, indicating that its positioning is impaired by the presence of aggresome-like structures (Fig 7B and C). However, ameliorating proteostasis through co-treatment with 4-PBA significantly restored the lateral positioning of the kinocilium in all HC rows (Fig 7B and C).

We next sought to test whether reducing the load of misfolded proteins during the development of Elp3cKO embryos could improve SGN survival and HC intrinsic polarity. Although daily injections of 4-PBA in dams, from E10.5 onwards, were not sufficient to prevent SGN loss (Appendix Fig S8), administration of the chemical chaperone from E13.5 onwards significantly improved the enrichment of LGN at the lateral edge of HC in Elp3cKO cochleae (Fig 7D). Furthermore, 4-PBA treatment significantly improved the peripheral positioning of the kinocilium in OHCs of Elp3cKO cochleae (Fig 7E and F). Altogether, these data confirm the importance of proteostasis to the proper establishment of HC intrinsic planar polarity in the developing mammalian OC.

Discussion

In this study, we show that the accumulation of misfolded proteins, via defective U_{34} tRNA modifications in the absence of Elp3, triggers the formation of aggresome-like structures in SGNs and cochlear HCs and impairs cochlear development and function. While post-mitotic neurons within the developing cochlea suffer from unresolved proteotoxicity and die by apoptosis, the epithelial HCs are able to overcome the survival threat but face bundle morphogenesis defects. The drastic failure of embryonic SGN survival is likely to be the major contributor to deafness in Elp3cKO mice. Although cochlear innervation is reduced at mature stages, afferent SGNs and synaptic contacts with HCs are still present. Hence, alterations in the stereociliary bundle shape and position could further aggravate the hearing function by reducing sound-induced stimulation of the remaining neurons. To the best of our knowledge, this work demonstrates for the first time the importance of developmental proteostasis to the establishment of the auditory function and highlights a novel link between proteome integrity and polarized processes.

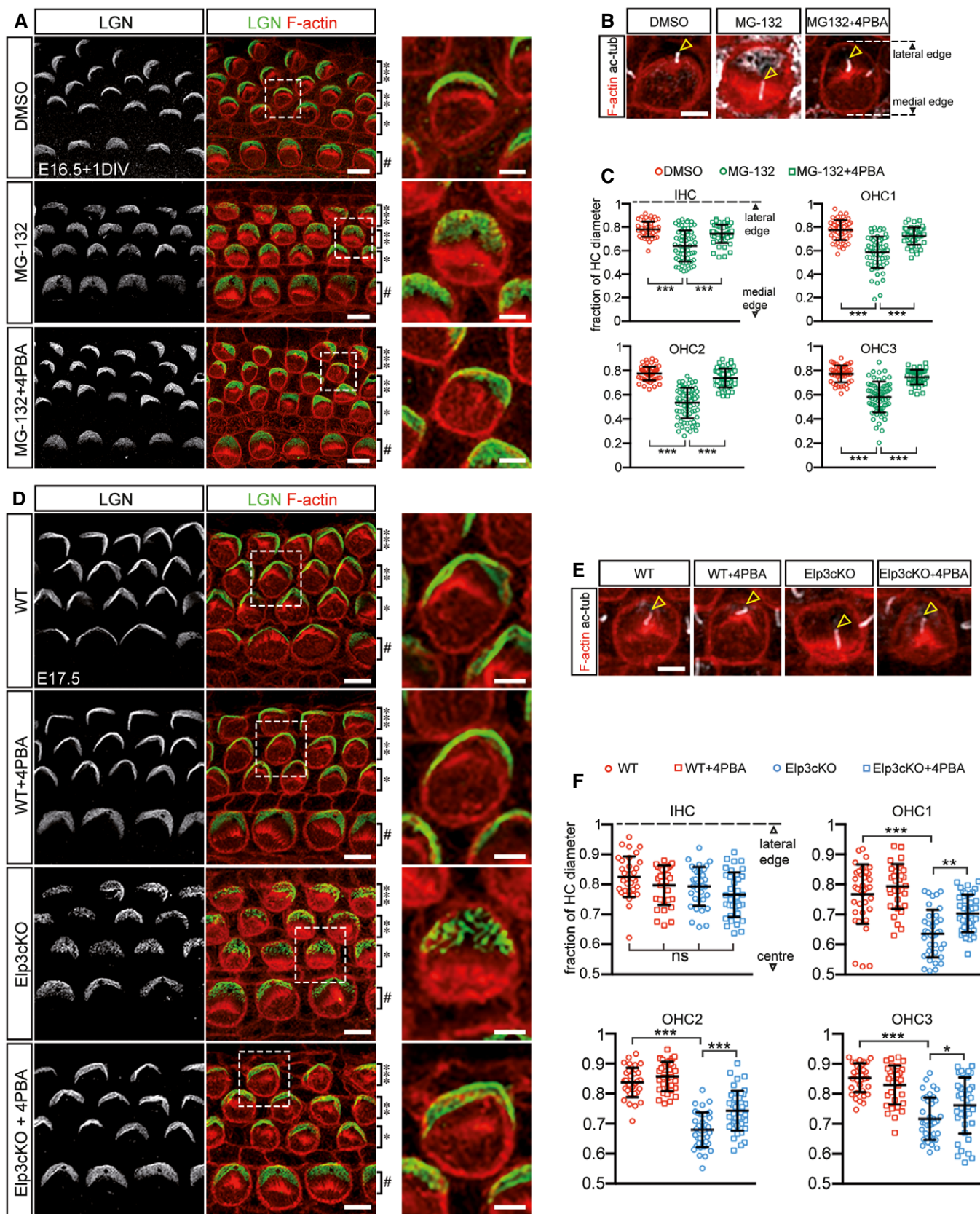


Figure 7.

Figure 7. Amelioration of proteostasis by 4-PBA treatment improves the establishment of intrinsic polarity in cochlear HCs.

A–C Intrinsic polarity is disrupted upon MG-132 treatment of cultured HCs and restored by the chemical chaperone 4-PBA. (A) LGN and F-actin immunostainings of E16.5 + 1DIV OCs reveal that MG-132 perturbs LGN distribution at the apical surface of HCs, while co-treatment with 4-PBA ameliorates its enrichment at the lateral edge. Scale bars = 5 μ m; magnified views = 2 μ m. (B) Acetylated alpha-tubulin immunostaining reveals that the kinocilium is centrally shifted by MG-132 and partially restored by 4-PBA in E16.5 + 1DIV HCs (yellow arrowheads = kinocilium base; scale bar = 2 μ m). (C) Kinocilium position plotted as a fraction of HC diameter for each HC row (DMSO/MG-132/MG-132 + 4PBA IHC: $n = 57/67/53$, $***P < 0.001$, $F = 34.52$, $DF = 2$; OHC1: $n = 61/66/53$, $***P < 0.001$, $F = 57.88$, $DF = 2$; OHC2: $n = 55/73/58$, $***P < 0.001$, $F = 124.7$, $DF = 2$; OHC3: $n = 48/66/43$, $***P < 0.001$, $F = 67.16$, $DF = 2$; pooled from 4 explants per condition; mean \pm SD; one-way ANOVA with Tukey's multiple comparisons test).

D–F *In vivo* administration of 4-PBA improves LGN localization and kinocilium position in Elp3cKO cochlear HCs. Pregnant mice were treated daily with saline or 4-PBA from E13.5, and the cochleae of WT and Elp3cKO embryos were analysed by immunostainings at E17.5. (D) The arc of lateral LGN enrichment remains in many Elp3cKO HCs after 4PBA administration. Scale bars = 5 μ m; magnified views = 2 μ m. (E) Acetylated alpha-tubulin immunostaining showing kinocilium position in WT or Elp3cKO OCs in the presence or absence of 4-PBA (yellow arrowheads = base of kinocilium; scale bar = 2 μ m). (F) Kinocilium position plotted as a fraction of HC diameter for each HC row (WT/WT + 4PBA/Elp3cKO/Elp3cKO + 4PBA IHC: $n = 35/31/35/36$, $P = 0.6812$, $F = 4.510$, $DF = 3$; OHC1: $n = 36/32/37/40$, $***P < 0.001$, $**P < 0.01$, $F = 27.60$, $DF = 3$; OHC2: $n = 35/33/38/42$, $***P < 0.001$, $F = 76.62$, $DF = 3$; OHC3: $n = 36/32/38/39$, $***P < 0.001$, $*P < 0.05$, $F = 27.86$, $DF = 3$; pooled from three animals per condition; mean \pm SD; one-way ANOVA with Tukey's multiple comparisons test).

Data information: #IHC; *OHC1; **OHC2; ***OHC3.

Disrupting proteostasis in developing SGNs triggers apoptosis

The increased apoptosis observed in embryonic Elp3cKO SGNs reveals their specific vulnerability to Elongator dysfunction and further emphasizes the prominent role of the complex during neurodevelopment. Neuronal death has been previously reported in Elongator mutants [29], but this is the first demonstration that aggresome-like structures are formed. Given that these juxtannuclear structures are present in the period preceding SGN death in Elp3cKO animals, and that aggresomes are typical hallmarks of neurodegenerative diseases [30], we believe that apoptosis is triggered by sustained proteotoxic stress. Aggresomes are not responsible for neuronal death *per se*, as they serve a cytoprotective role by limiting the toxic potential of misfolded proteins through sequestration and by facilitating their clearance through autophagy when proteasomal degradation is overwhelmed or dysfunctional [31,32]. The formation of aggresome-like structures upon otic *Elp3* knockdown is rather a strong indication that misfolded proteins are accumulating and that proteostasis is heavily disrupted. In Elp3-deficient SGNs, but not in HCs, the extent of misfolded proteins would reach a level that can no longer be resolved and would lead to apoptosis. This hypothesis is further supported by our demonstration that Chop and Chac1, which are factors involved in UPR-mediated apoptosis [3,23], are upregulated in E14 Elp3cKO cochleae.

Why neurons are particularly susceptible to protein misfolding and aggregation remains unclear, although it could be a result of higher rates of protein synthesis, reduced efficiencies of the protein quality control systems or differential activation of the various adaptive stress responses [21]. Accordingly, we found that protein aggregates are formed very early in SGNs during cochlear development and accumulate to such an extent that the aggresome-like structure distorts the cell nucleus. These features could explain why alleviation of protein misfolding by 4-PBA was not sufficient to induce a beneficial effect on Elp3cKO SGNs, while it was able to reduce the load of aggregates in HCs and improve the defects of intrinsic planar polarity.

While neuronal death has been extensively linked to protein misfolding and aggregation [30], it is also conceivable that SGN apoptosis results from compounded effects of Elongator deficiency. The stress generated by misfolded proteins may be exacerbated by translational defects of proteins specifically involved in neuron biology. Indeed, hypotranslation of neuropeptides and oxidative

stress-related proteins has been previously reported [33]. More recently, a proteomic analysis of Elp3-deficient dorsal root ganglion neurons showed a reduced translation rate of DNA damage repair proteins [34]. Given that neurons exhibit high metabolic rates and increased ROS production, particularly during their differentiation [35], they may have an elevated dependency on Elongator function for survival.

Accumulation of protein aggregates affects HC intrinsic polarity

We show that both Elp3 depletion and proteasome inhibition in HCs lead to an accumulation of protein aggregates that negatively interferes with kinocilium positioning and stereociliary bundle morphogenesis. LGN and $G\alpha_{13}$ proteins are still present in the lateral region of Elp3cKO HCs; however, they cover a larger domain that extends more medially, and they fail to exclude aPKC from the bare zone. As shown previously, such alterations result in flatter and centrally shifted bundles and may be accompanied by modest tissue planar polarity defects despite the normal localization of core PCP proteins [12,25,26,36]. Accordingly, neonatal Elp3cKO HCs display dysmorphic bundles as well as mild orientation defects, both of which could partially contribute to hearing loss. Although HC misorientation may be refined during postnatal stages, initial defects in polarity establishment have been associated with permanent sequelae in cochlear cell organization and function [37].

Since Elp3 deficiency causes codon-specific translational pausing and impaired protein folding [18], it is possible that one of the intrinsic polarity proteins could be a direct target for mistranslation. However, protein levels of LGN and $G\alpha_{13}$ are not affected by Elp3 loss, and we do not observe enrichment of those proteins within aggresome-like structures. Moreover, triggering the accumulation of naturally occurring misfolded species, through MG-132 treatment, recapitulates their mislocalization and impairs the positioning of the kinocilium at the HC apical surface. This implies that it is the presence of protein aggregates, *per se*, that disrupt the proper distribution of the intrinsic planar polarity proteins, regardless of the protein composition of the aggresome-like structures. This also raises the possibility that genetic mutations leading to the expression of an aggregation-prone moiety in HCs could potentially result in polarity defects in the developing cochlea.

There is growing evidence that LGN and other intrinsic polarity protein members can regulate cellular asymmetry in a range of

mitotic and non-mitotic cells, including endothelial cells [38], retinal progenitor cells [39] or glutamatergic neurons [40]. Thus, it will be interesting to investigate if compromised proteostasis also interferes with polarity in these structures. Interestingly, spindle orientation defects have already been observed in cortical apical progenitor division in the *Elp3*-deficient developing mouse brain [15].

Microtubule-based transport is susceptible to disruption of proteostasis

Our data demonstrate that the average speed of moving lysosomes is reduced upon either the loss of *Elp3* or following proteasome inhibition both in cochlear HCs and cultured HEK293T cells. Importantly, transport speed was partially recovered upon treatment with 4-PBA. Therefore, we propose that regulation of proteostasis may be necessary for normal microtubular trafficking and hence to ensure rapid and efficient delivery of intrinsic polarity proteins both at the lateral edge of HCs and at the cortical poles of dividing cells. As microtubule-based trafficking also governs cilium assembly and maintenance, this could also explain the ciliogenesis defects we observed in *Elp3*-deficient cells.

There are multiple mechanisms by which aggresome-like structures could impair transport. They could cause a physical block to intracellular transport, as previously suggested in neurodegenerative diseases [41]. Alternatively, they could disrupt the normal astral distribution of microtubules, reducing their transport capacity. There is evidence that intact astral microtubules are required for the enrichment of intrinsic polarity proteins at the cortices of dividing cells [42].

Aggresomes typically form in the vicinity of the microtubule-organizing centre (MTOC), which in HCs correspond to the basal body of the kinocilium at the most apical portion of the cell. We demonstrate that transport slowdown is restricted to this area, further emphasizing the link between the aggresome-like structures and microtubular transport perturbation. As suggested previously, a local reduction of transport around the MTOC could facilitate lysosomal clustering and subsequent degradation of aggregates by autophagy [28]. In addition, this apical restriction of transport defects may underlie the specificity of cargo proteins that display altered distribution. The delivery of $G\alpha_{13}$, LGN and aPKC to the most apical compartment of the HC would be hampered by the aggresomal traffic jam at the MTOC, whereas *Fz6*, which occupies more basal subcellular regions, is not affected by the presence of aggregates. Furthermore, it is logical to think that a reduction in transport speed would preferentially impact the localization of proteins displaying high turnover rates and implicated in highly dynamic processes, as shown for LGN and $G\alpha_i$ [43].

Protein quality control in hearing loss

In this study, we show the importance of protein quality control during cochlear formation, implying that mutations abolishing Elongator function or greatly reducing proteome integrity could be implicated in deafness. To the best of our knowledge, hearing impairments have not been reported in patients suffering from familial dysautonomia, a disease caused by mutations in the scaffolding subunit *Elp1*. However, the causal genetic mutations induce exon skipping and subsequent protein loss in a tissue-specific

manner, and whether *Elp1* gene mutations affect alternative splicing in the cochlea has yet to be determined. Similarly, it would be interesting to analyse whether the *Elp3* variants that are associated with an increased risk of developing amyotrophic lateral sclerosis (ALS) [44] are also linked to hearing impairments, especially as ALS pathophysiology includes intracellular protein aggregates, impaired ubiquitin-proteasomal degradation and disrupted axonal transport. Strikingly, a small pilot study revealed sensorineural hearing loss in 6/8 ALS patients [45].

The capacity of the protein quality control machinery to prevent or dispose of misfolded/aggregated proteins is known to decline with age [4]. To date, a causal link between proteome integrity and hearing loss has only been reported in ageing systems; impairment of the UPR pathway is associated with age-related hearing loss in mice [46], and the pharmacological upregulation of heat shock proteins can improve hearing function in a mouse model of presbycusis [47]. Our findings raise the possibility that genes encoding proteostasis regulators, such as tRNA-modifying enzymes, chaperones and players in the ubiquitin-proteasome and lysosome-autophagy systems could also be implicated in deafness with developmental origins. As such, extensive analysis of single nucleotide polymorphisms within this set of genes might reveal the existence of disease-modifying alleles that influence the onset or the severity of hearing loss.

Materials and Methods

Mouse lines and genotyping

Mice used in this study were time-pregnant WT (Janvier Labs, Saint-Berthevin, France), *FoxG1cre/+* [20] and *Elp3lox/lox* [15]. *FoxG1cre/+* and *Elp3lox/lox* mice were backcrossed in 129/Sv genetic background. All animals were housed under standard conditions and treated in accordance with guidelines provided by the Belgian Ministry of Agriculture, in agreement with the European Community Laboratory Animal Care and Use Regulations (2010/63/UE, 22 September 2010).

Cryosections

Fixed specimens were cryopreserved via overnight immersion in 20% sucrose solution in phosphate-buffered saline (PBS) at 4°C. Samples were washed briefly in a 1:1 solution of 20% sucrose and Cryochrome™ embedding resin (Thermo Fisher Scientific), then embedded in Cryochrome™ and frozen in liquid nitrogen. Frozen sections were cut using a Microm HM560 Cryostat and then mounted on Superfrost Plus™ slides (Thermo Fisher Scientific).

In situ hybridizations

In situ hybridizations were performed on 16- μ m cryosections as per Freeman et al [48]. Briefly, a 5' digoxigenin-labelled *Elp3* LNA probe: /5DigN/ATGAACTCCACCTTATCCACA (Exiqon, Denmark) was designed against exon 2 in order to discriminate between WT and *Elp3cKO*. Scramble LNA was used as a control. Probes were diluted in Hybridization Cocktail (VWR, Belgium) containing additional 50 mg/ml total yeast RNA (Merck, Belgium; R8759), 100 μ g/ml

heparin (Merck, Belgium; H3393) and Tween-20 0.25%. Hybridizations were performed at 65°C overnight. Excess probe was removed through serial washes in MABT (Maleic acid 100 mM; NaCl 150 mM, pH 7.8, Tween-20 0.25%). Anti-DIG-HRP (Merck, Belgium; 11093274910) was used at 1:2,000, and signal revelation was performed using NBT (Merck, Belgium; 11383213001)/BCIP (Merck, Belgium; 11383221001).

Antibodies

The following antibodies were used for immunostainings: rat Neurofilament H 1:1,000 (MAB5448 Millipore; RRID:AB_240862), mouse β III Tubulin 1:500 (MMS-435-P Covance; RRID:AB_2313773), rabbit Mafb 1:100 (NB600-266 Novus; RRID:AB_2137665), mouse Gata3 1:100 (558686 BD Biosciences; RRID:AB_2108590), rabbit cleaved caspase-3 1:200 (G7481 Promega; RRID:AB_430875), mouse Ctp2/Ribeye 1:250 (BD Transduction; RRID:AB_399431), rabbit GluR2/3 1:100 (Millipore AB1506; RRID:AB_90710), rabbit LGN 1:500 (kind gift from Dr. Fumio Matsuzaki, RIKEN CDB, Japan); rabbit Elp3 1:50 (D5H12, Cell Signaling; RRID:AB_11178379); mouse Frizzled-6 1:200 (AF1526, R&D Systems; RRID:AB_354842); rabbit Vangl2 1:200 (kind gift from Dr. Mireille Montcouquiol, Neuroscience Institute, Bordeaux, France); chicken $G\alpha_{i3}$ 1:100 (AB14246, Abcam; RRID:AB_301024); mouse Arl13b 1:200 (NIH NeuroMab clone N29B/66; RRID:AB_11000053); rabbit ALMS1 1:100 (kind gift from Dr. Tom Hearn, University of Southampton, UK); mouse acetylated α -tubulin 1:500 (T6793, Sigma; RRID:AB_477585); mouse gamma tubulin 1:500 (Abcam ab11316; RRID:AB_297920); and rabbit aPKC 1:100 (SC216, Santa Cruz Biotechnology; RRID:AB_2300359). For all primary antibodies, appropriate Alexa Fluor™ secondary antibodies were used for visualization. To visualize F-actin, Alexa Fluor™ Phalloidin 555 (Life Technologies, Belgium, A34055) and Alexa Fluor™ Phalloidin 647 (Life Technologies, Belgium, A22287) were used.

The following antibodies were used for Western blots: mouse Mono/Poly Ub conjugates 1:200 (clone FK2, Enzo Lifesciences; RRID:AB_10541840), rabbit Elp3 1:500 (D5H12, Cell Signaling; RRID:AB_11178379), rabbit LGN 1:500 (ab109594 Abcam; RRID:AB_10866713), rabbit $G\alpha_{i3}$ 1:500 (ab173527 Abcam, RRID:AB_2734141) and mouse β Actin–peroxidase 1:10,000 (A3854, Sigma, RRID:AB_262011).

Immunofluorescence

For whole-mount immunostainings, tissue was prepared by roughly dissecting otic capsules in cold PBS and immersing them in 4% paraformaldehyde (PFA) for 1 h at room temperature. After fine dissection of the cochlea, the tissue was permeabilized in PBS 0.3% Triton X-100 before blocking in PBS 0.3% Triton X-100 plus 10% normal donkey serum. Incubation with primary antibodies was done overnight at 4°C, in the presence of 10% normal donkey serum. Incubation with secondary antibodies was performed for 1 h at room temperature in the presence of 2% normal donkey serum. The tissues were washed three times for 30 min in PBS 0.3% Triton X-100 between antibody incubations. To detect LGN and $G\alpha_{i3}$, otic capsules were fixed in 1% paraformaldehyde for 45 min at 4°C before proceeding with the standard protocol. To detect LGN or $G\alpha_{i3}$ in organotypic explant cultures of the OC, fixation times in 1% PFA were reduced to 10 min at 4°C.

For immunostainings on cryosections, frozen sections were permeabilized in PBS 0.3% Triton X-100 for 15 min, before blocking in PBS 0.3% Triton X-100 with 10% normal donkey serum. Fresh blocking solution containing primary antibodies was added, and slides were incubated overnight at 4°C. Three 15-min washes in PBS 0.3% Triton X-100 were performed to remove excess primary antibody before a 1-h incubation of appropriate fluorescent secondary antibodies in PBS 0.3% Triton X-100. After a final set of three 15-min washes in PBS 0.3% Triton X-100, slides were mounted with a glass coverslip using Mowiol mounting medium. For Elp3, Gata3 and Mafb immunostainings, slides were pre-treated with citrate buffer (0.1 M sodium citrate pH 6.0) at 95°C for 5 min. For Elp3 staining, all washes and incubations were performed using TBS-Tween-20 1% and the blocking step used 10% BSA.

Auditory brainstem response

Hearing function was tested in an anechoic room on anesthetized P19 animals (isoflurane 2% in O₂), which were placed on a heating pad to maintain stable body temperature. Auditory brainstem responses were recorded with a SmartEP system (Intelligent Hearing systems, Miami, Florida) following Click stimuli. The hearing threshold was set as the minimal sound intensity that evoked a reproducible ABR waveform in the recorded electrical response and was averaged for both ears of each individual.

Scanning electron microscopy

Dissected cochleae were fixed in 2.5% glutaraldehyde in 0.1 M sodium cacodylate/3 mM CaCl₂ buffer (pH 7.3) for 2 h at room temperature. Samples were rinsed five times (10 min per rinse) in 0.1 M sodium cacodylate buffer and then fixed in 1% OsO₄ in 0.1 M sodium cacodylate buffer for 2 h at room temperature. Samples were rinsed in 0.1 M sodium cacodylate buffer and then rinsed in deionized water. Samples were then incubated in a saturated aqueous solution of 0.5% thiocarbohydrazide for 20 min, rinsed for 1 h in deionized water and then re-fixed in aqueous 1% OsO₄ for 1 h. After five rinses (10 min per rinse) with deionized water, the thiocarbohydrazide and subsequent steps were repeated. Samples were then serially dehydrated to dry 100% ethanol (series: 30, 50, 70, 85, 95, 100; 10 min per wash and then 2 × 10 min in dry 100% ethanol). Samples were then critical point dried with liquid CO₂, mounted and platinum coated in a Balzers SCD 030 sputtering unit (Balzers, Lichtenstein) using argon gas, 30 mA current and 30 mm distance. Observations were performed using an Environmental Scanning Electron Microscope (FEI ESEM-FEG XL-30, Philips, Netherlands).

Transmission electron microscopy

The samples were prepared as above (SEM). After dehydration at room temperature through a graded ethanol series, the samples were embedded in Epon for 48 h at 60°C. Ultrathin sections (80 nm) were obtained using an ultramicrotome (Reichert Ultracut E) with a diamond knife. Sections were mounted on copper/palladium grids, contrasted with uranyl acetate and lead citrate for 10 min and examined on a Jeol JEM-1400 microscope at 80 kV. Images were taken with a Quemesa Olympus camera.

Cell culture and siRNA transfection

HEK293T cells (ATCC-CRL-3216™) were used because of their high transfection efficiency and division rate and were tested negative for mycoplasma prior to use. Cells were seeded in 24-well plates and used the next day after reaching 50–60% confluency. Cells were treated with 1 μ M MG-132 (M7449, Sigma) with or without 1 mM sodium phenyl butyrate 4-PBA (SML0309, Sigma) during 7 h, and DMSO was kept constant at 0.1% for all conditions.

Specific endoribonuclease-prepared siRNA (MISSION esiRNA-hElp3 #EHU013421, esiRNA-hAlkbh8 #EHU086761, esiRNA-hElp1 (IKBKAP) #EHU156451, esiRNA-hElp5 #EHU070931 and esiRNA-Luc#EHURLUC) was mixed with Dharmafect (200 ng:1 μ l transfection reagent in 100 μ l OptiMEM per well) and added dropwise on cells in complete medium. Analysis was conducted 48 h after transfection with or without 1 mM 4-PBA for the last 18 h of culture.

Cochlea explant culture and treatments

E16.5 cochleae were dissected in cold HBSS + 25 mM HEPES. The organs of Corti were separated from the otic capsule and the lateral wall was removed, after which they were placed, sensory epithelium facing up, on coverslips which were pre-coated with polylysine (40 μ g/ml, Sigma) and laminin (6 μ g/ml, Sigma) overnight at 37°C. 130 μ l of DMEM/F12 (Thermo Fisher, Belgium) + 10% foetal bovine serum (FBS, Thermo Fisher, Belgium) was carefully dripped onto the coverslip, and the explants were cultured in humidified 37°C incubators with 5% CO₂.

Cochlea treatments were performed the next day, with 1 μ M MG-132 (M7449, Sigma) with or without 1 mM sodium phenyl butyrate 4-PBA (SML0309, Sigma) during 7 h, and DMSO was kept constant at 0.1% for all conditions. Experiments using Elp3cKO cochlear explants were performed by adding 1 mM 4-PBA to the plated explants and incubating for 18 h prior to analysis. The *in vivo* treatments of Elp3cKO animals were performed by intraperitoneal injections of saline or 200 mg/kg 4-PBA to pregnant females. For HC polarity experiments, injections were repeated daily from E13.5 to E16.5 and embryos were collected at E17.5 for analysis. For SGN survival experiments, injections were repeated daily from E10.5 up to birth.

Microtubular trafficking

LysoTracker Red™ (Thermo Fisher, Belgium) time-lapse movies were filmed on a Zeiss LSM880 confocal microscope. 120–140 frames were taken at intervals of 600 ms. Live cell cultures were kept in a Tokai Hit stage-top incubation chamber at a temperature of 37°C in the presence of 5% CO₂. HEK293T cells were cultured in 35/10 mm Cellview™ glass bottom four chambered culture dishes (Greiner), and time-lapse recordings were made from the dish. For time-lapse movies of the apical surface of the organ of Corti, coverslips harbouring the cochlea explants were placed inverted into a MaTek™ glass-bottomed 35-mm culture dish containing 400 μ l of DMEM/F12 + 10% FBS, so that the apical surface of the explant was adjacent to the glass bottom. Approximately 200 μ l of the culture medium was removed to create a mild surface tension between the inverted coverslip and the glass bottom, and time-lapse movies were acquired immediately afterwards. Lysosomal velocity

analysis was performed using the TrackMate™ plugin (v3.4.2) in ImageJ and the following settings: LOG detector; 1- μ m vesicular diameter; LAP tracker with a maximum distance of 2 μ m frame to frame; 1- μ m track segment gap closing; and a maximum frame gap of 3. All tracks were validated for accuracy and corrected where necessary using the TrackScheme portal within the TrackMate™ software.

Image acquisition and measurements

Confocal images were acquired using one of the following: Olympus FV1000, Nikon A1R or Zeiss LSM880 with Airyscan. All samples were processed identically, and the same cochlear position was imaged using the same exposure settings. Fluorescence intensity of LGN in dividing HEK293T cells was performed using the plot profile function in ImageJ. Plots were generated from lines drawn along the radius of the cell perpendicular to the division plane. Cell radii and fluorescence intensity measurements were converted to percentages, and mean fluorescence values were plotted as a function of % cell length. Measurements were restricted to cells dividing along the x-plane.

For Fz6/Vangl2 fluorescence intensity measurements, optical sections through the OC were combined in FIJI using a sum of slices projection. A threshold mask was created using the Otsu binarization algorithm, and integrated density of each localized region of Fz6/vangl2 enrichment was measured using the “3D Objects Counter” module.

Angles and rotation measurements

Measurements were conducted using maximum intensity projection images (40–60 \times magnification) taken in the basal region of cochleae stained with phalloidin and acetylated tubulin. The angle formed by the V-shaped bundle and its deviation from the medio-lateral axis were measured, using ImageJ, for 10–15 individual cells per row of HCs for six different animals per genotype. Data are presented as mean \pm SD for the bundle mean angle. Pooled data of stereociliary bundle deviation are presented in rose diagrams (using Oriana4 from Kovach Computing Services, Anglesey, UK) to visualize the overall distribution of bundle orientations. For Vangl2 and Fz6, protein localization was evaluated by measuring the angle formed between a line perpendicular to the medio-lateral axis and a line drawn from the cell centre to the middle of PCP protein domain (only for OHC2 and OHC3, which exhibit significant misorientation compared to controls). Pooled data obtained from three animals per genotype are plotted in rose diagrams, as described above.

Cilia length and position measurements

Cilia length was measured using the line tool in ImageJ, based on acetylated tubulin and Arl13b axoneme stainings. For transfected or treated HEK293T cells, images were taken randomly in each well at magnification 40 \times with a 2-fold zoom and maximum projection images were analysed. The data from 3 to 4 individual animals or cultures were pooled and presented as mean \pm SD.

For the analysis of postnatal samples, kinocilium position was determined in the basal turn of the cochlea by measuring the distance and angle of deviation from the cell centre to the basal

body. Pooled data are presented in a polar plot using Oriana4 (Kovach Computing Services, Anglesey, UK). For the analysis of embryonic stages, the diameter of each HC along the medio-lateral axis of the tissue and the distance of the kinocilium from the lateral edge of the cell were measured. From this, the position of the kinocilium was calculated as a fraction of the medio-lateral diameter of the HC and plotted as mean \pm SD.

Western blot

Cells were lysed on ice in RIPA extraction buffer (150 mM NaCl, 1% NP-40, 0.5% sodium deoxycholate, 0.2% SDS, 50 mM Tris, pH 8 and Protease Inhibitor Cocktail). Protein lysates were separated by 4–12% Tris-Bis gel electrophoresis in MES buffer (Novex, Life Science) and transferred onto PVDF membranes (Millipore) in transfer buffer (25 mM Tris, 190 mM glycine, 20% methanol). Non-specific binding was blocked with 5% dried fat-free milk in TTBS (50 mM Tris-HCl, pH 7.4, 150 mM NaCl, 0.1% Tween-20) or in PBS 0.05% Tween-20 (for LGN immunoblots) for 1 h at room temperature and incubated overnight at 4°C in the same solution with primary antibodies. After washing steps in TTBS or PBS 0.05% Tween-20, membranes were incubated with appropriate HRP-conjugated secondary antibody (1:5,000, Abcam) for 1 h at room temperature. Protein expression was detected by enhanced chemiluminescence (ECL, GE Healthcare). Protein loading was controlled by re-blotting the membrane with 1:10,000 anti- β Actin-peroxidase antibody (A3854, Sigma, RRID:AB_262011). The intensities were measured for each lane using ImageJ and normalized to the corresponding actin level.

Aggresome detection

HEK293T cells were cultured on poly-L-ornithine-coated cover slips, and the aggresome detection (PROTEOSTAT Aggresome Detection Kit, Enzo) was performed according to the manufacturer's recommendations. The same procedure was applied to dissected cochleae but the fixation time in PFA 4% (in Assay Buffer) was extended to 45 min. Co-staining with LGN or $G\alpha_{i3}$ was performed sequentially. First, cells were fixed for 5 min at 4°C in PFA 1% (in AB) and incubated with LGN or $G\alpha_{i3}$ antibodies as described above. After incubation with an AF647-conjugated secondary antibody, the cells were fixed for 30 min in PFA 4% (in AB) and the aggresome detection was performed.

RT-qPCR

Total RNA from HEK293T cells was extracted using TriPure Isolation Reagent (Roche) with a DNase I (Roche) step according to the manufacturer's instructions. cDNA was prepared from 1 μ g of RNA using the RevertAid H Minus First Strand cDNA Synthesis Kit (Fisher) and used for qPCR (1:20 cDNA dilution with 0.3 μ M of each primer and Faststart SYBR Green Master Mix, Roche) in a LightCycler 480 (Roche, Belgium). Expression levels were determined relative to the standard curve and normalized to the expression of GAPDH housekeeping gene. All amplifications were performed in triplicate, and six biological replicates coming from two independent experiments were analysed. PCR primer sequences are the following: hElp3forward 5'-CTA GAG ACA CCA ACA GGG GC-3',

hElp3reverse 5'-TCA GGC ATC ATA TGG GCC AC-3', hAlkbh8forward 5'-GCC GAA GCG GAG TTT GCT AT-3', hAlkbh8reverse 5'-CAC CAT TGG CAA CAA CCA GG-3', hElp1forward 5'-GGA CTG TGG GAG CTG ACT CT-3', hElp1reverse 5'-TCC CAC GAG ACA AGT ACA ACT-3', hElp5forward 5'-GAC GCG AGT TGG AGA TGT TG-3', hElp5reverse 5'-TCC CCA CAC AGT GCA GAT TT-3', hGadhforward 5'-GCA AAT TCC ATG GCA CCG T-3', hGadhreverse TCG CCC CAC TTG ATT TTG G; mChopforward: CCA CCA CAC CTG AAA GCA GAA; mChopreverse: AGG TGA AAG GCA GGG ACT CA; mChac1forward: CCG TGC TTG GTG GCT ATG; mChac1reverse: AGT GCT GTG AGG GGT TGG; mGAPDHforward: TGC AGT GGC AAA GTG GAG AT; mGAPDHreverse: TTT GCC GTG AGT GGA GTC ATA.

Statistical analyses

When possible, the sample size required to ensure adequate statistical power was determined *a priori* by using G*power software (www.gpower.hhu.de). Most of the statistical analyses were performed using the GraphPad Prism™ (GraphPad) software. Details of individual tests, *n* numbers and *P*-values are given in the figure legends. Data were tested for normality before applying statistical analyses, and appropriate parametric (ANOVA or *t*-test) or non-parametric (Kruskal–Wallis or Mann–Whitney) tests were performed depending upon the outcome. For the analysis of circular data, the distribution was tested using the Watson U^2 test using Oriana4 (Kovach Computing Services, Anglesey, UK) and the length of mean vectors was analysed using *t*-tests. Unless otherwise stated, experiments depicted by representative images were performed on at least three independent occasions. Where possible, data acquisition and analyses were performed by different researchers and analyses were performed blind.

Expanded View for this article is available online.

Acknowledgements

We thank the GIGA-Research technology platforms (Imaging: Sandra Ormene and Jean-Jacques Goval). We thank the animal facility staff for help with mouse colony maintenance. We thank Dr. Philippe Compère for technical assistance with the scanning electron microscopy experiments. We thank Dr. M. Montcouquiol and Dr. F. Matsuzaki for kindly providing reagents. We thank Dr. I. Gladwyn-Ng, Dr. E. Peyre, Dr. L. Cordon-Barros and A. Even for critical discussions. We are indebted to B. Minguet for his help with illustrations.

Author contributions

SF, SMS, LD and BM designed the study. SF, SMS and LD phenotyped the Elp3cKO mouse, performed *in situ* hybridizations, immunohistochemistry, biochemistry and data analysis. SF and LD performed cell and tissue culture. SF performed time-lapse recordings. RP contributed to aggresome detection assays, cilium length and lysotracker analysis. NT and MT performed TEM experiments. NT performed SEM experiments. GM, LVH and SL provided some Elp3cKO embryos. LN and AC shared mouse models and reagents, and provided critical input on the results. KH and P-BVL provided technical assistance. BM contributed to data analysis and interpretation. SF, LD and BM wrote the article.

Conflict of interest

The authors declare that they have no conflict of interest.

References

1. Oishi N, Duscha S, Boukari H, Meyer M, Xie J, Wei G, Schrepfer T, Roschitzki B, Boettger EC, Schacht J (2015) XBP1 mitigates aminoglycoside-induced endoplasmic reticulum stress and neuronal cell death. *Cell Death Dis* 6: e1763
2. Wong E, Cuervo AM (2010) Integration of clearance mechanisms: the proteasome and autophagy. *Cold Spring Harb Perspect Biol* 2: a006734
3. Hetz C, Chevet E, Oakes SA (2015) Proteostasis control by the unfolded protein response. *Nat Cell Biol* 17: 829–838
4. Kaushik S, Cuervo AM (2015) Proteostasis and aging. *Nat Med* 21: 1406–1415
5. Delacroix L, Malgrange B (2015) Cochlear afferent innervation development. *Hear Res* 330: 157–169
6. Ezan J, Montcouquiol M (2013) Revisiting planar cell polarity in the inner ear. *Semin Cell Dev Biol* 24: 499–506
7. Seifert JR, Mlodzik M (2007) Frizzled/PCP signalling: a conserved mechanism regulating cell polarity and directed motility. *Nat Rev Genet* 8: 126–138
8. Goodrich LV, Strutt D (2011) Principles of planar polarity in animal development. *Development* 138: 1877–1892
9. Wang Y, Nathans J (2007) Tissue/planar cell polarity in vertebrates: new insights and new questions. *Development* 134: 647–658
10. Peyre E, Jaouen F, Saadaoui M, Haren L, Merdes A, Durbec P, Morin X (2011) A lateral belt of cortical LGN and NuMA guides mitotic spindle movements and planar division in neuroepithelial cells. *J Cell Biol* 193: 141–154
11. Segalen M, Johnston CA, Martin CA, Dumortier JG, Prehoda KE, David NB, Doe CQ, Bellaiche Y (2010) The Fz-Dsh planar cell polarity pathway induces oriented cell division via Mud/NuMA in *Drosophila* and zebrafish. *Dev Cell* 19: 740–752
12. Tarchini B, Jolicoeur C, Cayouette M (2013) A molecular blueprint at the apical surface establishes planar asymmetry in cochlear hair cells. *Dev Cell* 27: 88–102
13. Hudspeth AJ, Jacobs R (1979) Stereocilia mediate transduction in vertebrate hair cells (auditory system/cilium/vestibular system). *Proc Natl Acad Sci USA* 76: 1506–1509
14. Otero G, Fellows J, Li Y, de Bizemont T, Dirac AM, Gustafsson CM, Erdjument-Bromage H, Tempst P, Svejstrup JQ (1999) Elongator, a multisubunit component of a novel RNA polymerase II holoenzyme for transcriptional elongation. *Mol Cell* 3: 109–118
15. Laguesse S, Creppe C, Nedialkova DD, Prevot PP, Borgs L, Huysseune S, Franco B, Duysens G, Krusy N, Lee G et al (2015) A dynamic unfolded protein response contributes to the control of cortical neurogenesis. *Dev Cell* 35: 553–567
16. Huang B, Johansson MJ, Bystrom AS (2005) An early step in wobble uridine tRNA modification requires the Elongator complex. *RNA* 11: 424–436
17. Johansson MJ, Esberg A, Huang B, Bjork GR, Bystrom AS (2008) Eukaryotic wobble uridine modifications promote a functionally redundant decoding system. *Mol Cell Biol* 28: 3301–3312
18. Nedialkova DD, Leidel SA (2015) Optimization of codon translation rates via tRNA modifications maintains proteome integrity. *Cell* 161: 1606–1618
19. Nguyen L, Humbert S, Saudou F, Chariot A (2010) Elongator – an emerging role in neurological disorders. *Trends Mol Med* 16: 1–6
20. Hebert JM, McConnell SK (2000) Targeting of cre to the Foxg1 (BF-1) locus mediates loxP recombination in the telencephalon and other developing head structures. *Dev Biol* 222: 296–306
21. Lim J, Yue Z (2015) Neuronal aggregates: formation, clearance, and spreading. *Dev Cell* 32: 491–501
22. Johnston JA, Ward CL, Kopito RR (1998) Aggresomes: a cellular response to misfolded proteins. *J Cell Biol* 143: 1883–1898
23. Mungrue IN, Pagnon J, Kohannim O, Gargalovic PS, Lusic AJ (2009) CHAC1/MGC4504 is a novel proapoptotic component of the unfolded protein response, downstream of the ATF4-ATF3-CHOP cascade. *J Immunol* 182: 466–476
24. Jones C, Roper VC, Foucher I, Qian D, Banizs B, Petit C, Yoder BK, Chen P (2008) Ciliary proteins link basal body polarization to planar cell polarity regulation. *Nat Genet* 40: 69–77
25. Sipe CW, Lu X (2011) Kif3a regulates planar polarization of auditory hair cells through both ciliary and non-ciliary mechanisms. *Development* 138: 3441–3449
26. Ezan J, Lasvaux L, Gezer A, Novakovic A, May-Simera H, Belotti E, Lhoumeau AC, Birnbaumer L, Beer-Hammer S, Borg JP et al (2013) Primary cilium migration depends on G-protein signalling control of subapical cytoskeleton. *Nat Cell Biol* 15: 1107–1115
27. Couwenbergs C, Labbe JC, Goulding M, Marty T, Bowerman B, Gotta M (2007) Heterotrimeric G protein signaling functions with dynein to promote spindle positioning in *C. elegans*. *J Cell Biol* 179: 15–22
28. Zaarur N, Meriin AB, Bejarano E, Xu X, Gabai VL, Cuervo AM, Sherman MY (2014) Proteasome failure promotes positioning of lysosomes around the aggresome via local block of microtubule-dependent transport. *Mol Cell Biol* 34: 1336–1348
29. Chaverra M, George L, Mergy M, Waller H, Kujawa K, Murnion C, Sharples E, Thorne J, Podgajny N, Grindeland A et al (2017) The familial dysautonomia disease gene IKBKAP is required in the developing and adult mouse central nervous system. *Dis Models Mech* 10: 605–618
30. Taylor JP, Hardy J, Fischbeck KH (2002) Toxic proteins in neurodegenerative disease. *Science* 296: 1991–1995
31. Kawaguchi Y, Kovacs JJ, McLaurin A, Vance JM, Ito A, Yao TP (2003) The deacetylase HDAC6 regulates aggresome formation and cell viability in response to misfolded protein stress. *Cell* 115: 727–738
32. Taylor JP, Tanaka F, Robitschek J, Sandoval CM, Taye A, Markovic-Plese S, Fischbeck KH (2003) Aggresomes protect cells by enhancing the degradation of toxic polyglutamine-containing protein. *Hum Mol Genet* 12: 749–757
33. Fernandez-Vazquez J, Vargas-Perez I, Sanso M, Buhne K, Carmona M, Paulo E, Hermand D, Rodriguez-Gabriel M, Ayte J, Leidel S et al (2013) Modification of tRNA(Lys) UUU by elongator is essential for efficient translation of stress mRNAs. *PLoS Genet* 9: e1003647
34. Goffena J, Lefcort F, Zhang Y, Lehrmann E, Chaverra M, Felig J, Walters J, Buksch R, Becker KG, George L (2018) Elongator and codon bias regulate protein levels in mammalian peripheral neurons. *Nat Commun* 9: 889
35. Agostini M, Romeo F, Inoue S, Niklison-Chirou MV, Elia AJ, Dinsdale D, Morone N, Knight RA, Mak TW, Melino G (2016) Metabolic reprogramming during neuronal differentiation. *Cell Death Differ* 23: 1502–1514
36. Bhonker Y, Abu-Rayyan A, Ushakov K, Amir-Zilberstein L, Shivatzki S, Yizhar-Barnea O, Elkan-Miller T, Tayeb-Fligelman E, Kim SM, Landau M et al (2016) The GPSM2/LGN GoLoco motifs are essential for hearing. *Mamm Genome* 27: 29–46
37. Copley CO, Duncan JS, Liu C, Cheng H, Deans MR (2013) Postnatal refinement of auditory hair cell planar polarity deficits occurs in the absence of Vangl2. *J Neurosci* 33: 14001–14016
38. Wright CE, Kushner EJ, Du Q, Bautsch VL (2015) LGN directs interphase endothelial cell behavior via the microtubule network. *PLoS One* 10: e0138763

39. Lacomme M, Tarchini B, Boudreau-Pinsonneault C, Monat C, Cayouette M (2016) The LGN protein promotes planar proliferative divisions in the neocortex but apicobasal asymmetric terminal divisions in the retina. *Development* 143: 575–581
40. Sans N, Wang PY, Du Q, Petralia RS, Wang YX, Nakka S, Blumer JB, Macara IG, Wenthold RJ (2005) mPins modulates PSD-95 and SAP102 trafficking and influences NMDA receptor surface expression. *Nat Cell Biol* 7: 1179–1190
41. Strom AL, Gal J, Shi P, Kasarskis EJ, Hayward LJ, Zhu H (2008) Retrograde axonal transport and motor neuron disease. *J Neurochem* 106: 495–505
42. Siegrist SE, Doe CQ (2005) Microtubule-induced Pins/Galphai cortical polarity in *Drosophila* neuroblasts. *Cell* 123: 1323–1335
43. Zheng Z, Wan Q, Liu J, Zhu H, Chu X, Du Q (2013) Evidence for dynein and astral microtubule-mediated cortical release and transport of Galphai/LGN/NuMA complex in mitotic cells. *Mol Biol Cell* 24: 901–913
44. Simpson CL, Lemmens R, Miskiewicz K, Broom WJ, Hansen VK, van Vught PW, Landers JE, Sapp P, Van Den Bosch L, Knight J et al (2009) Variants of the elongator protein 3 (ELP3) gene are associated with motor neuron degeneration. *Hum Mol Genet* 18: 472–481
45. Philippou E, Joubert K (2013) The audiological profile and perceptions of hearing loss in individuals with Amyotrophic Lateral Sclerosis. In *Amyotrophic Lateral Sclerosis: Symptoms, Treatment and Prognosis*, Segawa K, Ijichi R (eds), pp 1–10. Hauppauge, NY: Nova Science publishers
46. Wang W, Sun Y, Chen S, Zhou X, Wu X, Kong W, Kong W (2015) Impaired unfolded protein response in the degeneration of cochlea cells in a mouse model of age-related hearing loss. *Exp Gerontol* 70: 61–70
47. Mikuriya T, Sugahara K, Sugimoto K, Fujimoto M, Takemoto T, Hashimoto M, Hirose Y, Shimogori H, Hayashida N, Inouye S et al (2008) Attenuation of progressive hearing loss in a model of age-related hearing loss by a heat shock protein inducer, geranylgeranylacetone. *Brain Res* 1212: 9–17
48. Freeman SD, Keino-Masu K, Masu M, Ladher RK (2015) Expression of the heparan sulfate 6-O-endosulfatases, Sulf1 and Sulf2, in the avian and mammalian inner ear suggests a role for sulfation during inner ear development. *Dev Dyn* 244: 168–180